COMPARISON OF DATA FROM THE TRANSIT TIME VELOCIMETER WITH OTHER SYSTEMS NOW IN USE FOR VELOCITY MEASUREMENT

W. T. Mayo, Jr. and A. E. Smart

SPECTRON DEVELOPMENT LABORATORIES, INC.
3303 HARBOR BOULEVARD, SUITE G-3
COSTA MESA, CALIFORNIA 92626

May 1979

Final Report for Period January 1978 — September 1978

Prepared for

ARNOLD ENGINEERING DEVELOPMENT CENTER/DOTR
ARNOLD AIR FORCE STATION, TENNESSEE 37389

NOTICES
When U. S. Government drawings, specifications, or other data are used for any purpose other than a definitely related Government procurement operation, the Government thereby incurs no responsibility nor any obligation whatsoever, and the fact that the Government may have formulated, furnished, or in any way supplied the said drawings, specifications, or other data, is not to be regarded by implication or otherwise, or in any manner licensing the holder or any other person or corporation, or conveying any rights or permission to manufacture, use, or sell any patented invention that may in any way be related thereto.
Qualified users may obtain copies of this report from the Defense Documentation Center.
References to named commerical products in this report are not to be considered in any sense as an indorsement of the product by the United States Air Force or the Government.

This final report was submitted by Spectron Development Laboratories, Inc., 3303 Harbor Boulevard, Suite G-3, Costa Mesa, California 92626, under contract F40600-78-C-0002 with Arnold Engineering Development Center/DOTR, Air Force Systems Command, Arnold Air Force Station, Tennessee 37389. Mr. Marshall K. Kingery, DOTR, was the Air Force Project Manager.

This report has been reviewed by the Information Office (OI) and is releasable to the National Technical Information Service (NTIS). At NTIS, it will be available to the general public, including foreign nations.

APPROVAL STATEMENT

This report has been reviewed and approved.

Marshall K. Kingery

MARSHALL K. KINGERY
Project Manager, Research Division
Directorate of Test Engineering

Approved for publication:

FOR THE COMMANDER

Robert W. Crossley

ROBERT W. CROSSLEY, Lt Colonel, USAF
Acting Director of Test Engineering
Deputy for Operations

REPORT DOCUMENTATION PAGE

READ INSTRUCTIONS BEFORE COMPLETING FORM

1 REPORT NUMBER: AEDC-TR-79-32	2 GOVT ACCESSION NO.
3 RECIPIENT'S CATALOG NUMBER	
4 TITLE (and Subtitle): COMPARISON OF DATA FROM THE TRANSIT TIME VELOCIMETER WITH OTHER SYSTEMS NOW IN USE FOR VELOCITY MEASUREMENTS	5 TYPE OF REPORT & PERIOD COVERED: Final Report - Jan 1978 - Sep 1978
	6 PERFORMING ORG REPORT NUMBER
7 AUTHOR(s): W. T. Mayo, Jr. and A. E. Smart	8 CONTRACT OR GRANT NUMBER(s): F40600-78-C-0002
9 PERFORMING ORGANIZATION NAME AND ADDRESS: Spectron Development Laboratories, Inc. 3303 Harbor Boulevard, Suite G-3 Costa Mesa, California 92626	10 PROGRAM ELEMENT, PROJECT, TASK AREA & WORK UNIT NUMBERS: Program Element 65807F
11 CONTROLLING OFFICE NAME AND ADDRESS: Arnold Engineering Development Center/OIS Air Force Systems Command Arnold Air Force Station, Tennessee 37389	12 REPORT DATE: May 1979
	13 NUMBER OF PAGES: 86
14 MONITORING AGENCY NAME & ADDRESS (if different from Controlling Office)	15 SECURITY CLASS. (of this report): UNCLASSIFIED
	15a DECLASSIFICATION DOWNGRADING SCHEDULE: N/A

16 DISTRIBUTION STATEMENT (of this Report)

Approved for public release; distribution unlimited.

17 DISTRIBUTION STATEMENT (of the abstract entered in Block 20, if different from Report)

18 SUPPLEMENTARY NOTES

19 KEY WORDS (Continue on reverse side if necessary and identify by block number)

lasers
laser velocimeters
measuring instruments
measurement
velocity

20 ABSTRACT (Continue on reverse side if necessary and identify by block number)

This report discusses the principles of operation of the laser transit anemometer (LTA), developed and constructed under this contract, and its use with a photon correlator. AEDC developed an electronic processor for fringe laser velocimeter systems. A test was conducted in a free jet with a stationary Mach disc to compare the sensitivity of the new processor with the older Model 8 burst-counter processor with respect to small-particle relaxation behind

DD FORM 1 JAN 73 1473 EDITION OF 1 NOV 65 IS OBSOLETE

20. ABSTRACT (Continued)

a shock front. The LTA combined with the photon correlator produced acceptable velocity data. Flare light can be most satisfactorily rejected by well-considered geometrical design and attention to optical components. The transit configuration allows at least an order of magnitude improvement in the proximity to walls at which good measurements may be made. The capabilities of the transit system to look at smaller particles and measure stresses by spot radiation are especially useful close to walls.

AFSC
Arnold AFB Tenn

PREFACE

The work reported herein was conducted by the Spectron Development Laboratories, Inc., Costa Mesa, California under contract F40600-78-C-0002 with the Arnold Engineering Development Center, Air Force Systems Command. Air Force Project Manager for this contract was Marshall K. Kingery, AEDC/DOTR. The work was conducted between January and September 1978, and the manuscript for this report was submitted to AEDC on 23 February 1979.

The reproducibles used in the reproduction of this report were supplied by the authors.

TABLE OF CONTENTS

TABLE OF CONTENTS (CONT'D.)

LIST OF FIGURES

LIST OF FIGURES (CONT'D.)

SECTION 1.0

INTRODUCTION

1.1 BACKGROUND

A laser transit anemometer (LTA), combined with photon-limited pulse discriminators and digital correlation signal processing, offers a high probability for measuring fluid velocities under some adverse conditions where presently used fringe laser velocimeter systems are inadequate. Specifically, the LTA is likely to be superior for measurements near a wall or in the boundary layer of a model. The surface scatter and reflected light is so great that conventional fringe LV systems are "blinded" with high noise or photodetector overload; however, the superior flare rejection capabilities of a properly designed LTA system can allow operation closer to the surfaces. The LTA furnishes mean velocity magnitude and direction to high accuracy in the plane normal to the incident beams. The same data may be processed to yield two dimensional turbulence intensity information on a statistical basis.

Some cases exist at AEDC where velocimeter applications are needed and where numerous particles are contained in the flow, but they are too small for successful operation of the fringe type of velocimeter. The photon correlator combined with the transit time anemometer will be far more likely to produce acceptable velocity data under these conditions.

High velocities in some applications may be more suitable measured with an LTA system.

1.2 CONTRACT OBJECTIVE

The objective of this work was to demonstrate the principles of the laser transit anemometer and its use with a photon correlator. The AEDC had recently developed a new electronic processor for fringe LV systems and scheduled a test in a free jet with a stationary Mach disc to compare sensitivity of the new processors with the older Model 8 burst-counter processor. The LTA system constructed under this contract under the direction of Mr. Marshall Kingery, AEDC, was to be demonstrated simultaneously with the AEDC fringe system to obtain some measure of the relative sensitivity of the LTA with respect to small-particle relaxation behind a shock front.

1.3 HISTORICAL AND RELATED REFERENCES

Initial laser velocimeter (LV) experiments in this country were made with heterodyne (reference beam) optical systems using frequency tracking electronics. The dual-beam (fringe) optical systems and classical-signal burst-counter electronics have proven to be more applicable to high-speed air flows and have been used with success at the AEDC and elsewhere.

Particle lag problems are sometimes encountered in aerodynamic LV measurements[1,2]. Unseeded (or even filtered) air contains a very large number of submicron particles which are sufficiently small to follow high accelerations in the flow*, but obtaining adequate back-scatter single-particle signal-to-noise ratios for classical burst-counter measurements is difficult even with the higher powered argon lasers.

---

*W. T. Mayo has reported measurements of large numbers of particles in the 0.2 - 0.8 micrometer diameter range in the laboratory air at the AEDC[3,4].

In the late 60's, the idea of a time of flight laser velocimeter was discussed at the AEDC (private communication, J. D. Trolinger), and published by Thompson and Tanner[5,6] at Queens University, Belfast. Schodl[7] and others at DFVLR developed certain specific techniques for implementation of transit anemometry. A. E. Smart reported measurements with a different implementation of a transit anemometry system in 1977 (Reference 11). The advantages of such systems include much less total probe volume and much higher focused laser beam intensity than typical fringe LV systems produce, and both of these qualities enhance sensitivity to small particles while decreasing the probability of intercepting the more sparsely distributed large particles. In addition, the higher resolution spatial filtering provides much better background light (flare) rejection when measurements near bodies are desired.

Photon correlation has been known to be ideally more sensitive than classical detection for several years. The techniques and theory for fringe LV systems are reviewed in References 4, 8-13. Unfortunately, the available correlator electronic speed has not really been adequate* to be compatible with transonic speeds and the simultaneous demands for small probe volumes. An LTA system has a great advantage here. It achieves lower electronic bandwidth requirements while increasing the small-particle SNR and isolation. The reduced bandwidth makes the use of a 50 nsec correlator feasible for supersonic velocities. Thus, the combination of two-spot techniques and digital correlation offers exceptional improvements in small-particle sensitivity and is practical at supersonic velocities.

A. E. Smart, formerly of Rolls-Royce, Derby, England, has taken advantage of these compatible techniques (two-spot and digital correlation) and extended them in some rather clever ways[11-12]. He designed, constructed and used a system employing a small helium neon laser to

*John Abbiss has made supersonic measurements at the R.A.E. in England but with large fringe spacing appropriate for the 50 nsec resolution of the Malvern Instruments correlator[10].

make backscatter measurements in both subsonic flows and supersonic flows. The details of the Rolls-Royce instrument, which is capable of mapping out the two-dimensional u-v velocity probability function for statistically stationary flows, are proprietary to Rolls-Royce and have not been released. However, Dr. Smart later joined SDL and assisted W. T. Mayo in the design and construction of a new argon-laser transit anemometer system during the execution of the AEDC contract reported herein.

In previous NASA, AEDC and ARPA sponsored research, W. T. Mayo, Jr. has developed extensive laser velocimeter computer simulation and design software[15-17] and photon correlation interpretation software[18]. The experience and software have been used for calculations reported in the next section.

1.4 SCOPE

During the period January 1978 through September 1978, Spectron Development Laboratories personnel including and under the direction of A. E. Smart and W. T. Mayo have designed, constructed, modified, and demonstrated a new LTA system which includes not only significant novel advances in optical and mechanical technique, but also in system sensitivity theory and computation, electronic detection techniques, and microcomputer techniques for experiment control and data acquisition and display. This system was transported to the AEDC in September 1978 and used successfully in comparative unseeded free jet trials with an AEDC fringe LV system.

This report describes the sensitivity of laser transit anemometry, the experimental hardware constructed under this contract, and the results of the measurements at the Arnold Center. More recent transonic backscatter measurements made at NASA Ames with the same equipment will be reported elsewhere.

SECTION 2.0

SYSTEM SENSITIVITY COMPUTATIONS

The outstanding advantages of the laser transit anemometry over fringe laser velocimetry include the increased sensitivity to submicron particles in high-speed flow and the improved rejection of flare light from surfaces. These two features enable a well-designed LTA system to make backscatter transonic and supersonic flow measurements through windows and near models and other surfaces. In order to theoretically quantify and predict expected performance as an aid to engineering selection of required laser power and other optical parameters, we have performed computer simulation computations. Also, the wall flare rejection of a co-annular transceiver optical system has been examined. The results of these studies are presented here.

2.1 COMPARATIVE COMPUTER SIMULATION OF TRANSIT ANEMOMETER AND FRINGE VELOCIMETER SIGNALS

Spectron Development Laboratories has a set of fringe laser velocimeter computer simulation programs which have been written over the past three years for NASA Langley[17], the Naval Underwater Systems Center, the Advanced Research Projects Agency[15], and under SDL private funds[16]. We have modified two of these programs slightly to allow simulation of a single spot system with no fringes and with one-half the total available laser power. We have simulated a single-particle signal from 0.3 μm diameter particles with velocity 400 m/sec through the center of the probe volume of comparable fringe and transit anemometer systems.

Figure 1 illustrates the geometry of the coaxial transmitter/receiver objective lens with the dimensions of the $1/e^2$ Gaussian spot diameters as shown. Table 1 lists the input and output system parameters of the two systems.

We have assumed that the signals are produced with a photomultiplier tube (PMT) whose single photoelectron pulse response is a triangular pulse 5 nsec wide at its half height. The PMT is assumed to have a Gaussian pulse height distribution with 25 percent rms standard deviation (an excellent tube). The PMT output signals are then filtered by a Gaussian bandpass filter in the fringe case or a Gaussian low-pass filter in the one-spot case. The filter response characteristics are plotted in Figure 2. As indicated by Table 1, we considered both the conditions of zero background light and that of 10^{10} photoelectrons/second.

Figure 3 is the classical fringe velocimeter signal from the 0.3 μm diameter particle with the amplitude given in photoelectrons/second. Figure 4 is the output of the photomultiplier tube. Figure 5 is the output of the bandpass filter. As we can see, the peak mean photo-electron rate is approximately $5x10^7$, so this signal would be totally swamped by large background light. Figure 6 illustrates the classically expected pulse from the single spot. Figure 7 shows the PMT output, and Figure 8 shows the results of filtering. Figures 9, 10, and 11 depict the same signal in the presence of 10^{10} photoelectrons/second background light.

It is much more likely that one will obtain a high background from flare when using the fringe system (with a 260 μm diameter pinhole in the receiver) than when using a two-spot system (2 pinholes each at 10.6 μm diameter). Thus, the two-spot system produces large signal-to-noise ratio advantages for single signals in three ways: the filter for the two-spot can be nearly the same bandwidth as the intrinsic signal bandwidth without the necessity of having a tracking filter; the two-spot has higher intensity signals by a factor equal to the

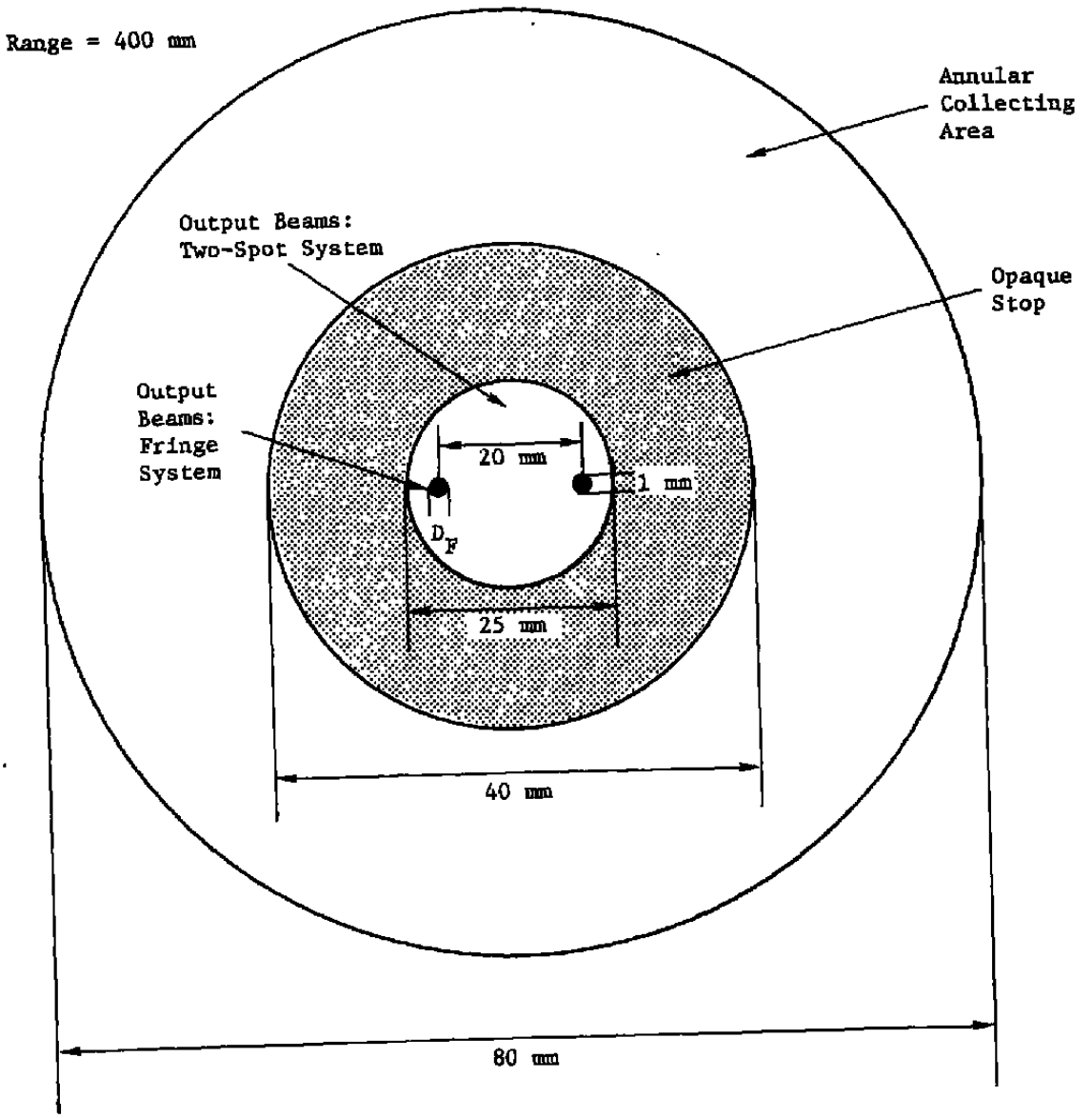

Figure 1. Dimensions of Transmitter Beams and Receiver Annulus.

Table 1. System Parameters.

Parameter	Two-Spot	Fringe Velocimeter
System		
Wavelength	514.5 nm	514.5 nm
Laser Power	0.5 watt/spot	1 watt
Optical Efficiency	0.3	0.3
Detector Quantum Efficiency	0.2	0.2
Transmitted Beam Diameter	25 mm	1 mm
Range	400 mm	400 mm
Beam Separation at Transmitter	0.5 mm $\approx$ 0	20 mm
No. of $1/e^2$ Fringes	0	25
Probe Volume Spot Diameter	10.6×10^{-6} m	N/A
Signal Frequency	N/A	38.9 MHz
Probe Volume Width	N/A	262×10^{-6} m
Single Burst Duration	26.6×10^{-9} s	0.655×10^{-6} s
Particle		
Velocity	400 m/sec	400 m/sec
Index of Refraction	1.5+j0	1.5+j0
Diameter	0.3×10^{-6}	0.3×10^{-6}
Background Light		
Two Levels:	zero and 10^{10} photoelectrons/sec (equivalent to 20 nw optical power collected by phototube)	

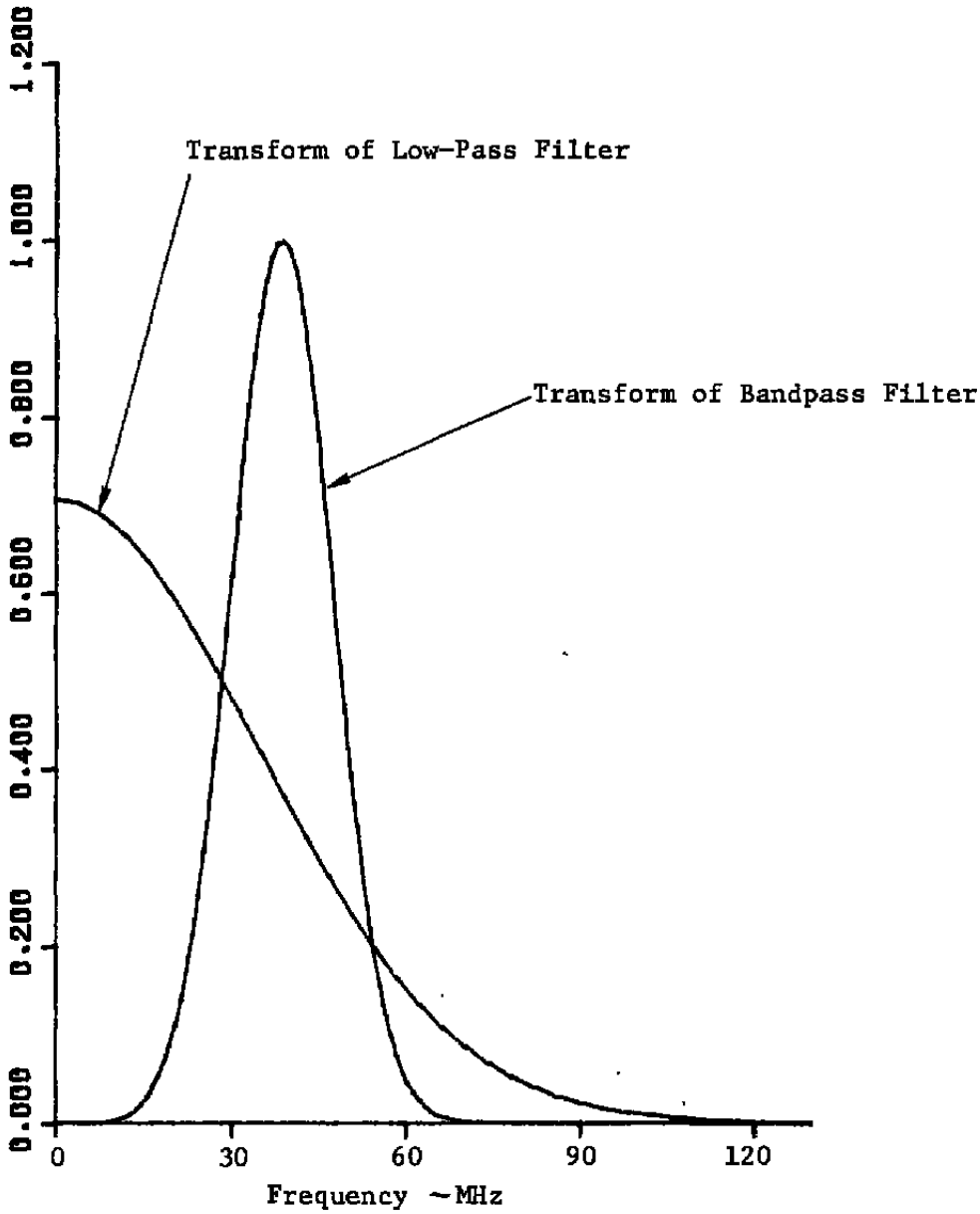

Figure 2. Filter Characteristics.

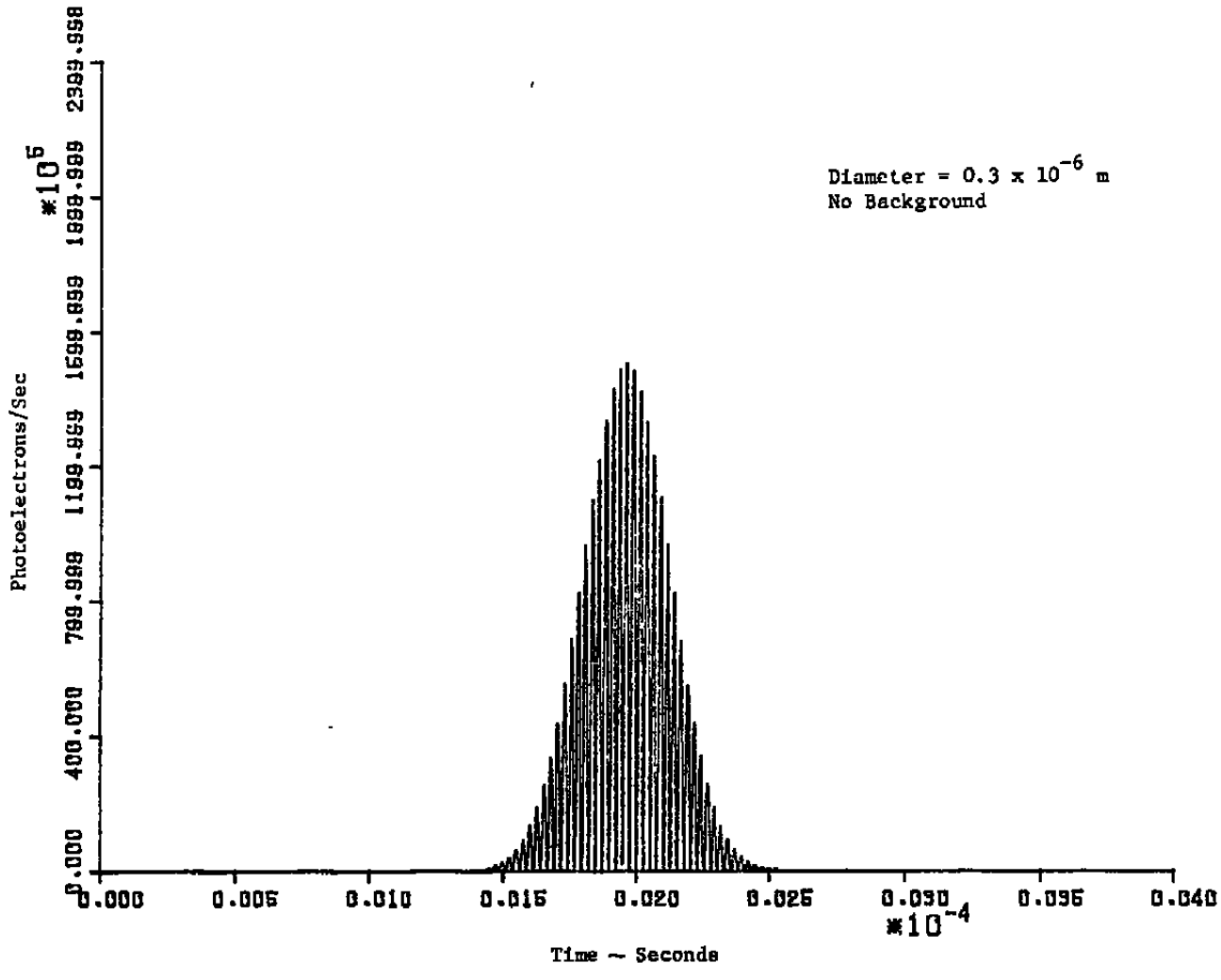

Figure 3. Classical Signal, Fringe Velocimeter, 0.3×10^{-6} m Diameter.

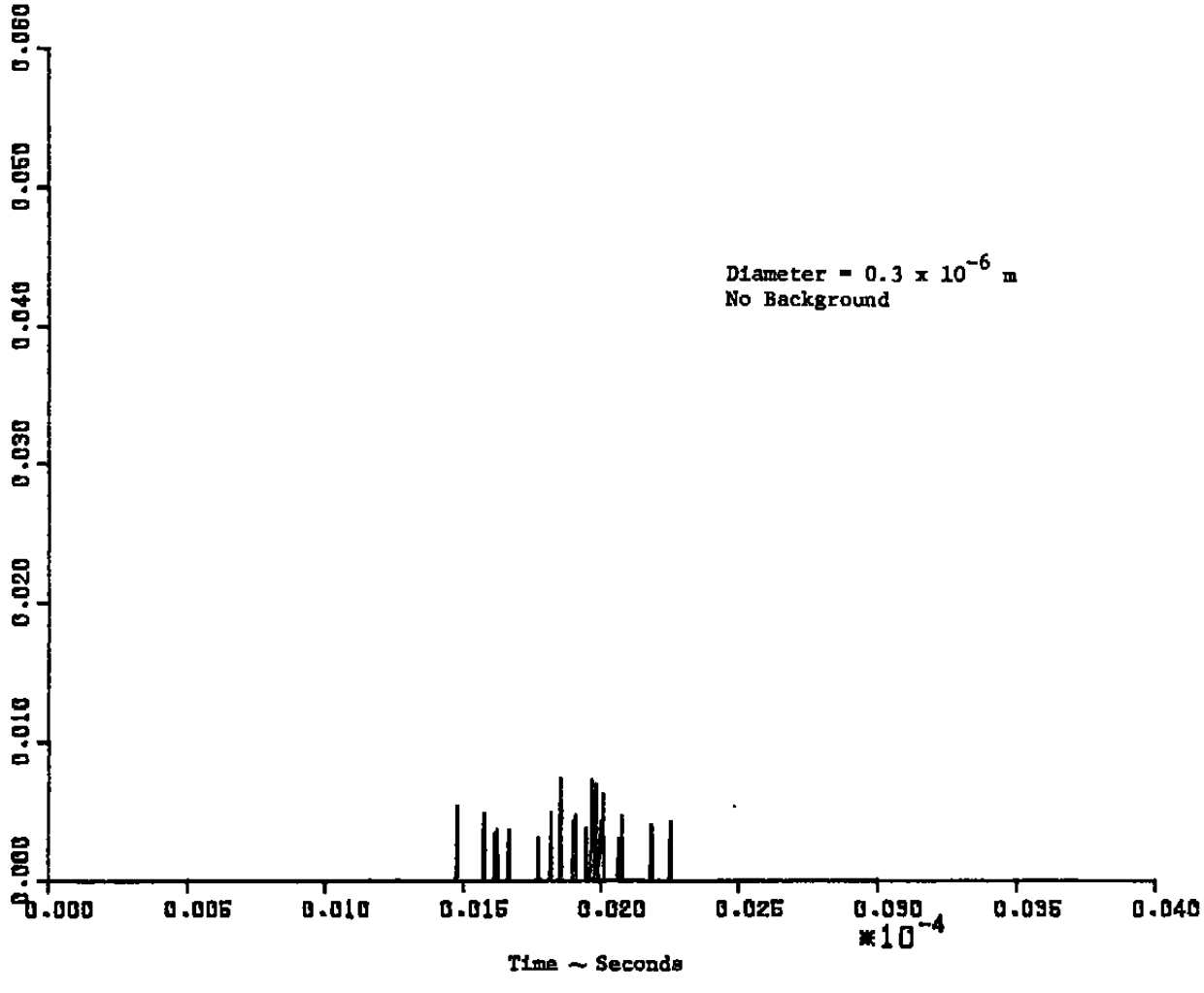

Figure 4. Actual PMT Signal from PMT, Fringe Case.

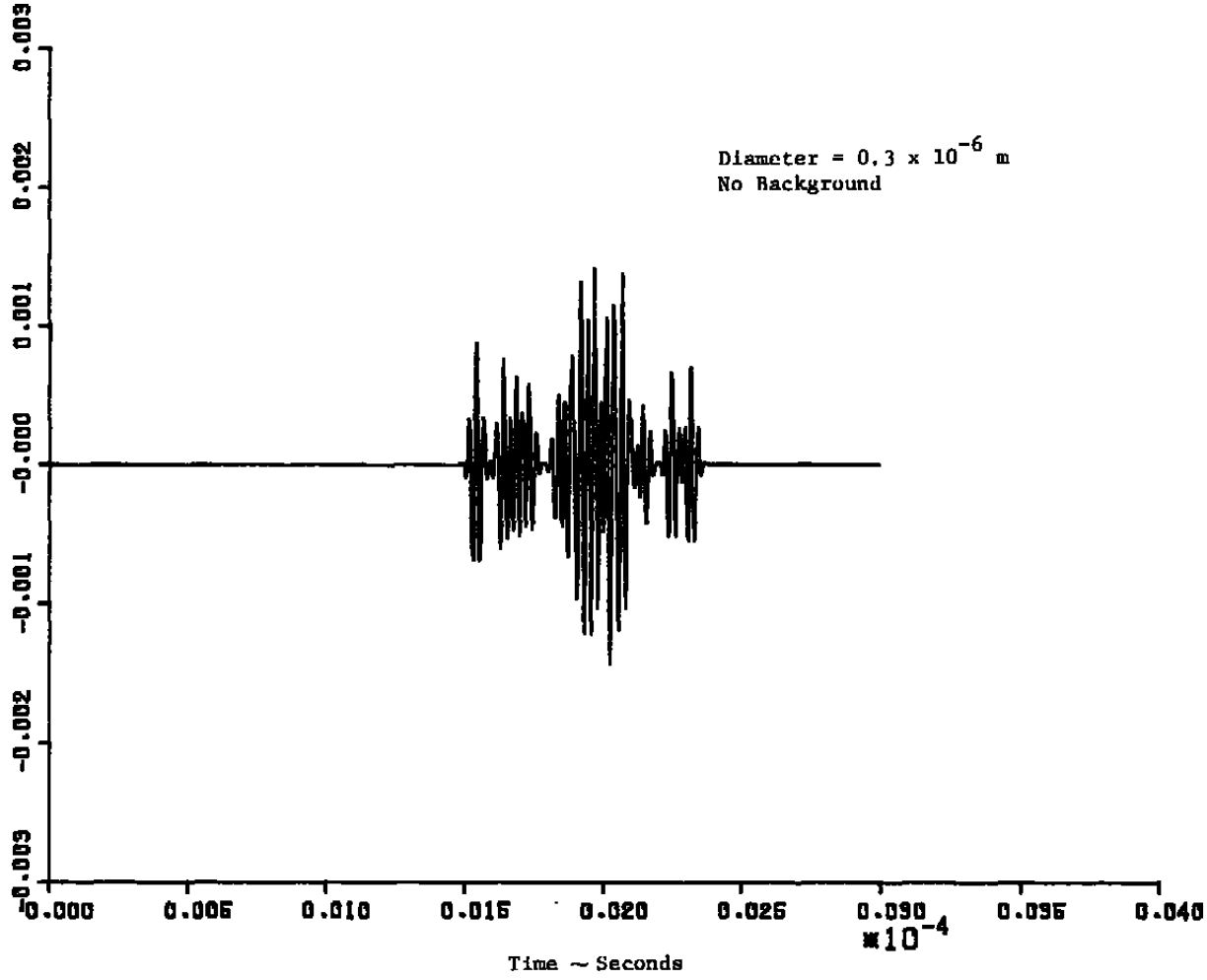

Figure 5. Filtered Output from Fringe Case.

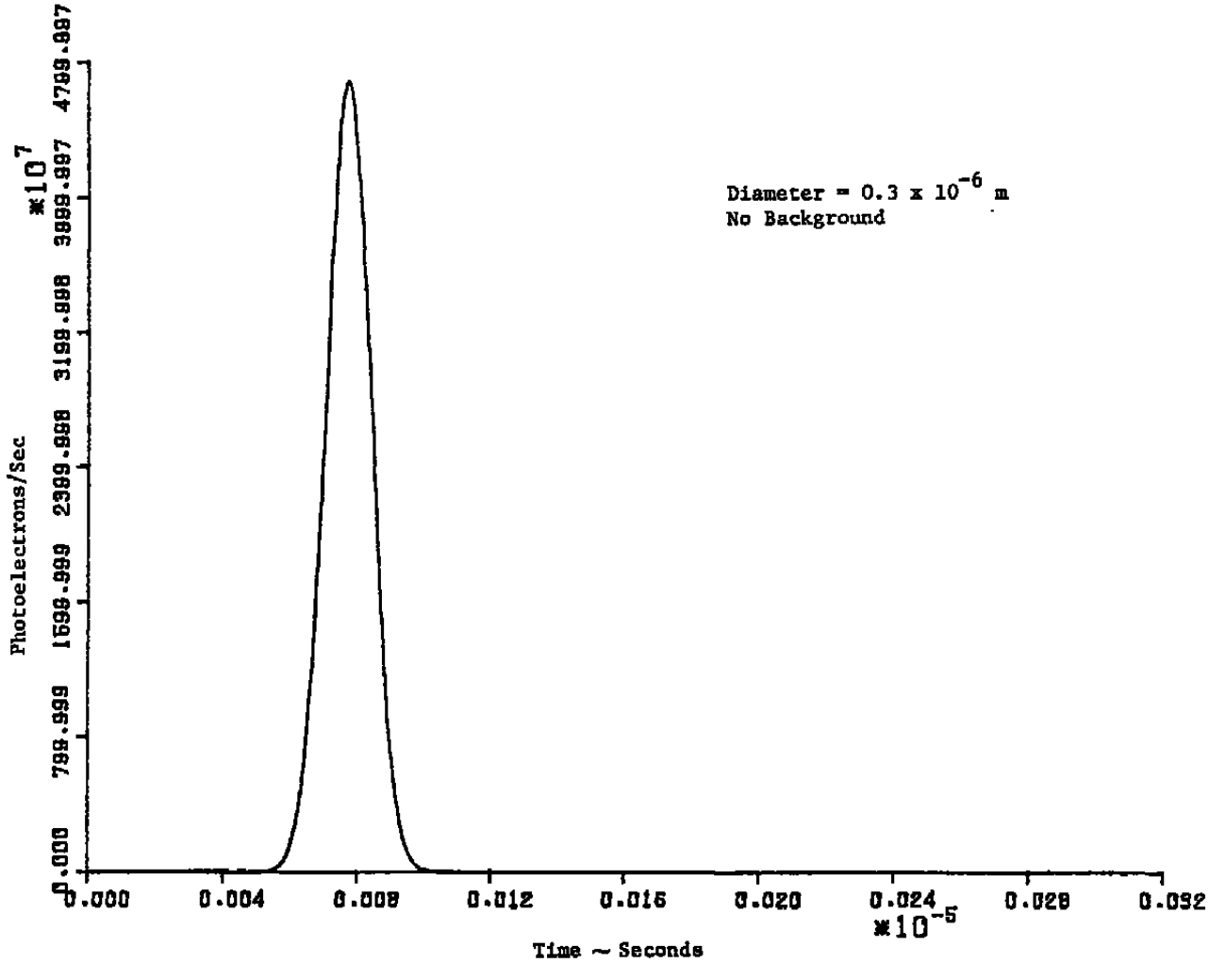

Figure 6. Classical Output, Transit Velocimeter.

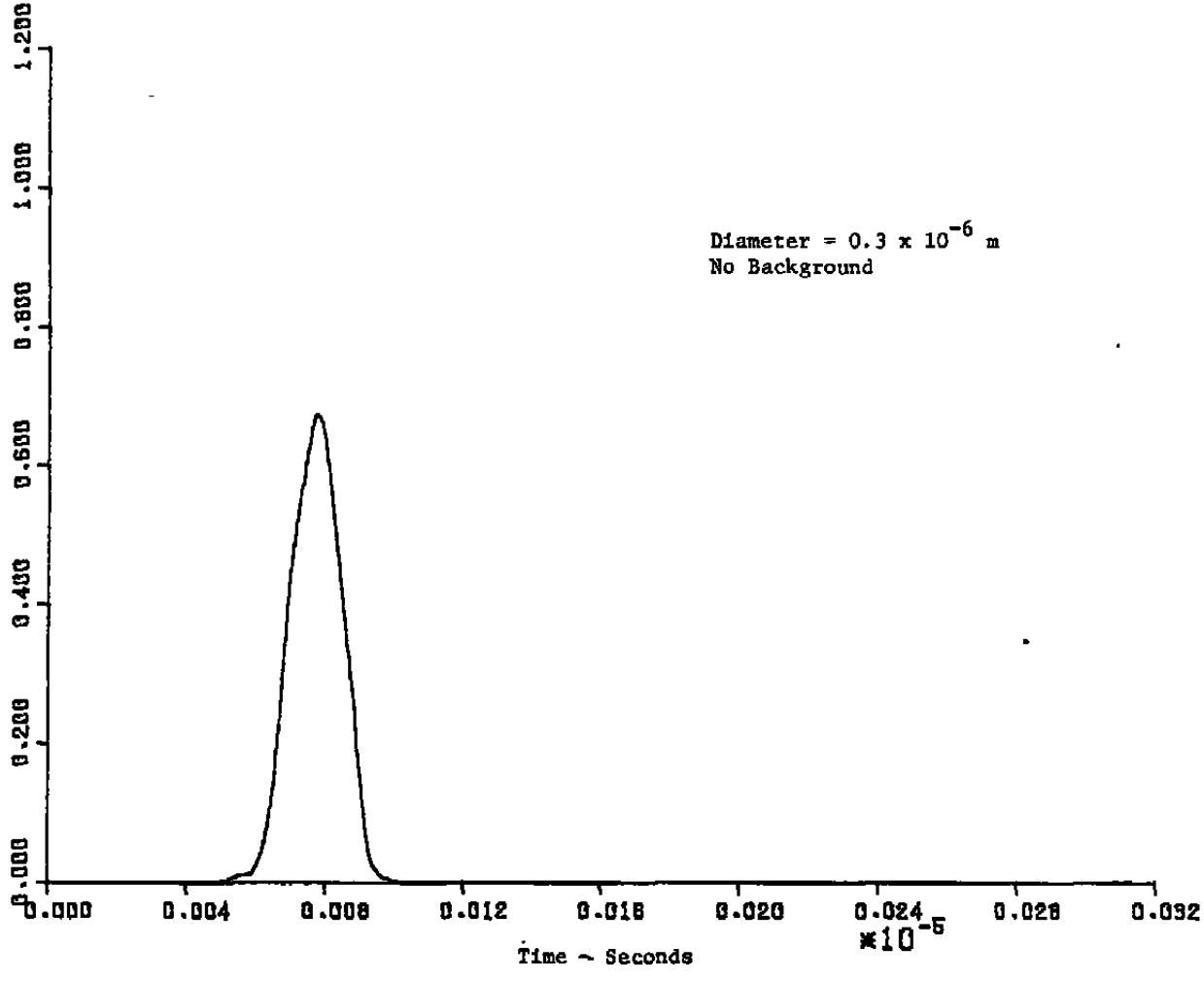

Figure 7. Photomultiplier Output, Transit Velocimeter.

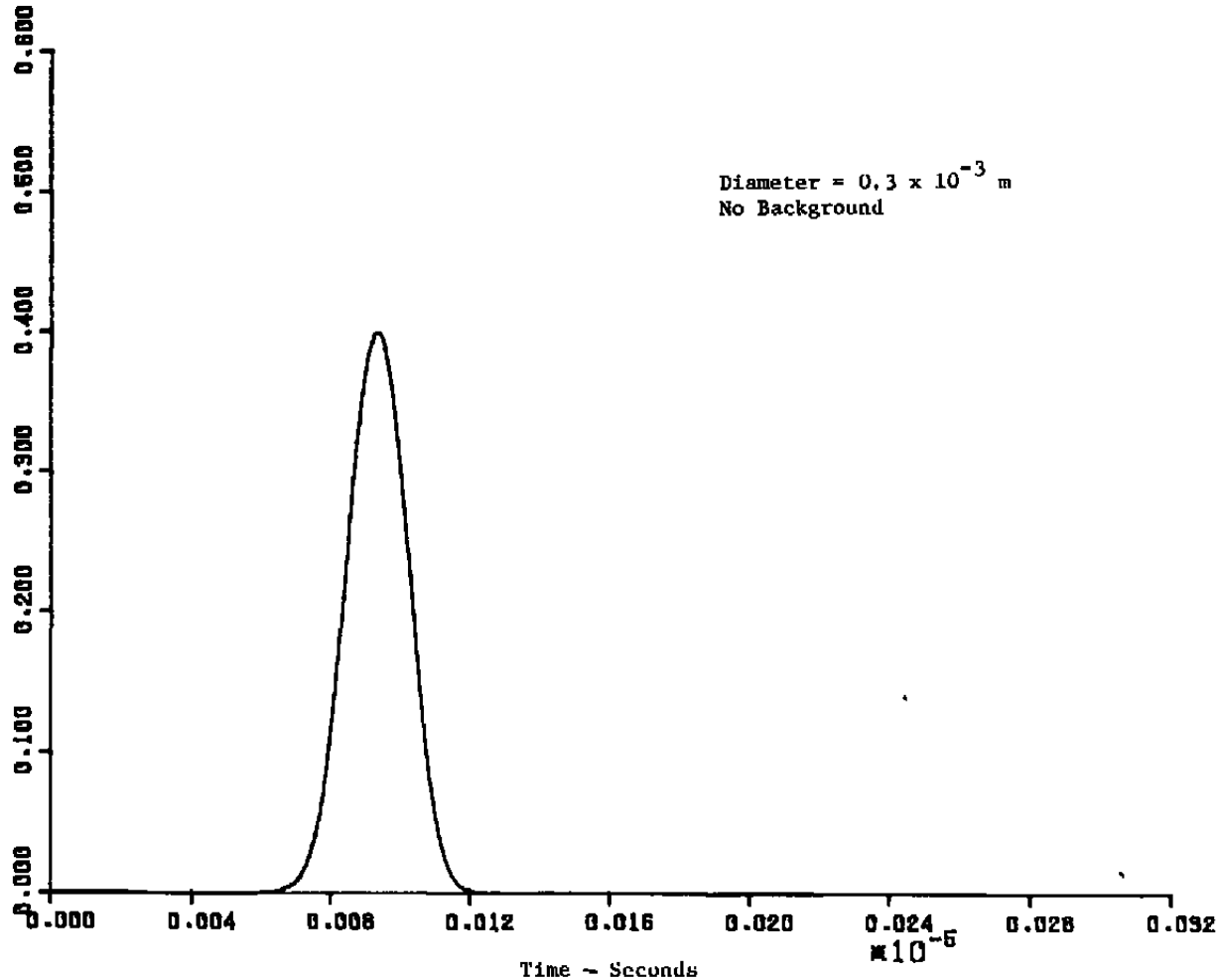

Figure 8. Filtered Signal, Transit Velocimeter.

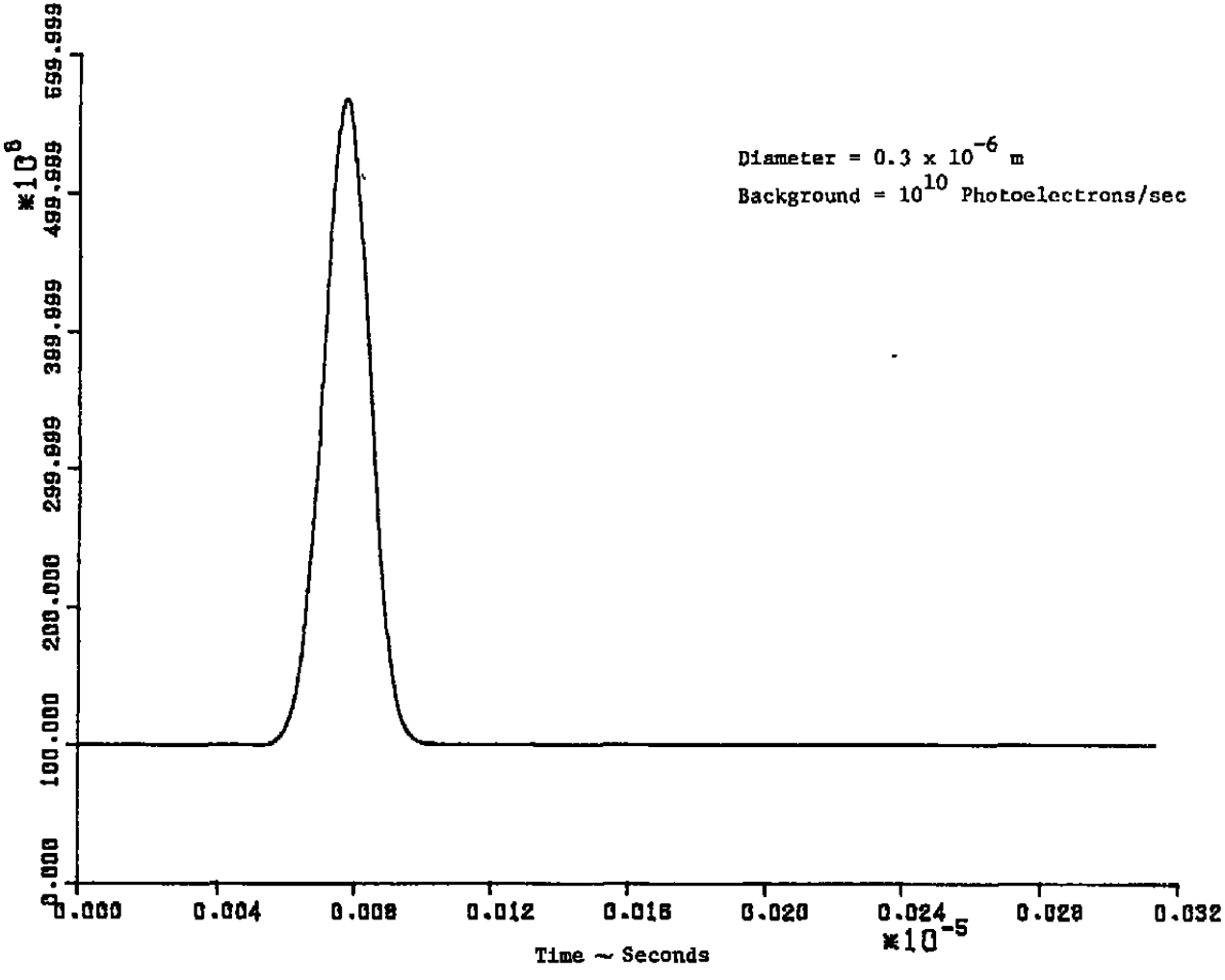

Figure 9. Transit Velocimeter, Classical Signal, Plus Background.

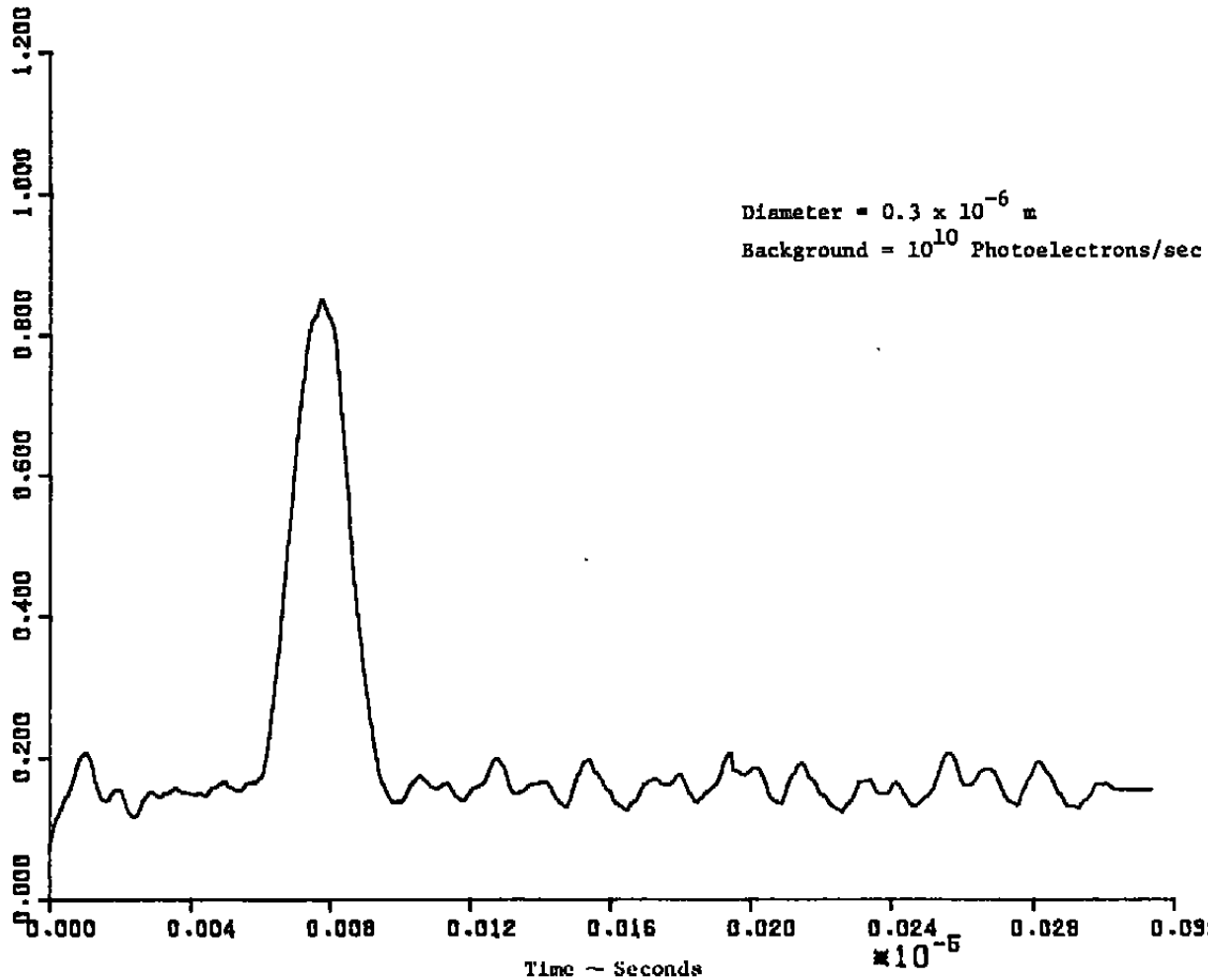

Figure 10. Phototube Output, Transit Velocimeter.

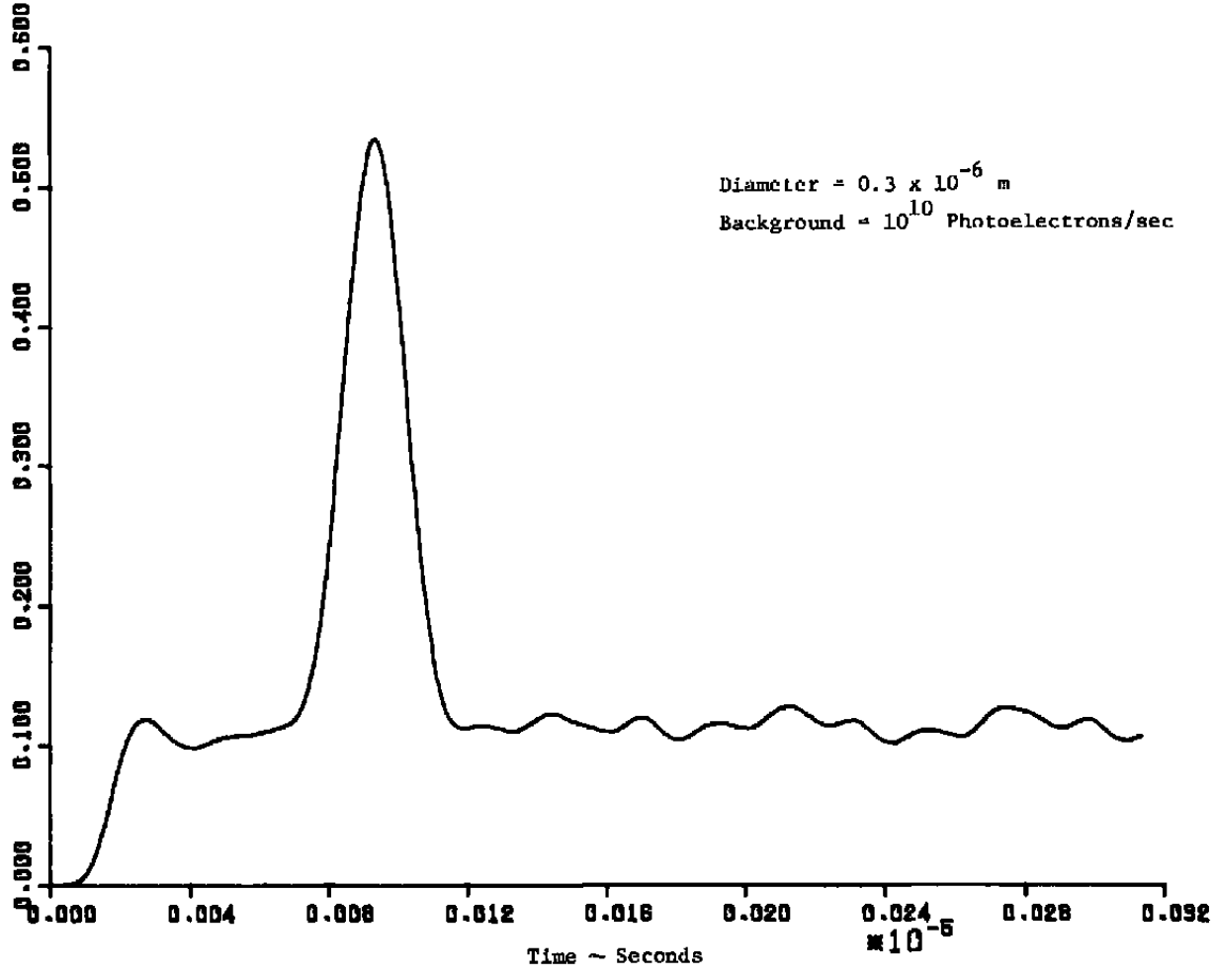

Figure 11. Filtered Signal, Transit Velocimeter.

square of the ratio of the beam radii at the probe volume; the background light which will get through the pinhole spatial filter is much less for the two-spot system due to the smaller apertures. On the negative side, all optical aberrations, including those introduced by windows and turbulent index of refraction effects, will enlarge the achievable spot size and reduce the advantage of a transit velocimeter system.

The simulation results have indicated that there is no need to use a 1 watt argon laser beam if good optics are used. It is easy to see that aberrations can destroy the advantage of a higher power laser. We anticipate that a 200 mw laser will be adequate for most transit anemometer applications at short ranges.

Most of the material in this section was included along with additional discussion in reference (13).

2.2 WALL FLARE REJECTION

The ability of a laser transit anemometer system to reject flare light from model or other surfaces has been analyzed and discussed briefly by A. E. Smart and presented verbally at the Dynamic Flow Conference 1978, Baltimore, Maryland. A brief paper written for that conference is included here as Appendix A. The analysis shows that with typical optical system parameters, an LTA system may approach walls more closely than fringe LV systems by approximately an order of magnitude. However, aberrations can nullify much of the theoretical advantages unless attention is given to optical and mechanical detail.

SECTION 3.0

HARDWARE
SYSTEM DESCRIPTION

3.1 OVERVIEW

We begin in this subsection with a system overview and proceed in later subsections to describe specific subsystem engineering considerations. Figure 12 is an interconnection diagram which illustrates schematically the separate physical units which comprise the experimental system. The dashed line indicates which units are located 15 meters from the optical head. Figures 13, 14 and 15 are photographs which show a perspective view of the experimental optical head and the optical and electronic components inside the head. The optical and electronic subsystems inside the head are listed in Tables 2 and 3 for future reference.

It is apparent that there are several major functions of the subsystem components which include: production and manipulation of laser light, detection, signal conditioning, fast (correlator) signal processing, signal monitoring, rotation control, subsystem sequence control, data acquisition, display and processing.

3.2 MICROPROCESSOR CONTROL, DATA MANAGEMENT AND DISPLAY

The conduct of meaningful experimental measurements requires many rapidly repetitive sequential operations, significant bookkeeping and data collection, and graphic presentation of data to the operator in near real time for verification of proper system performance. Small computer systems are now ideally suited in price and performance for

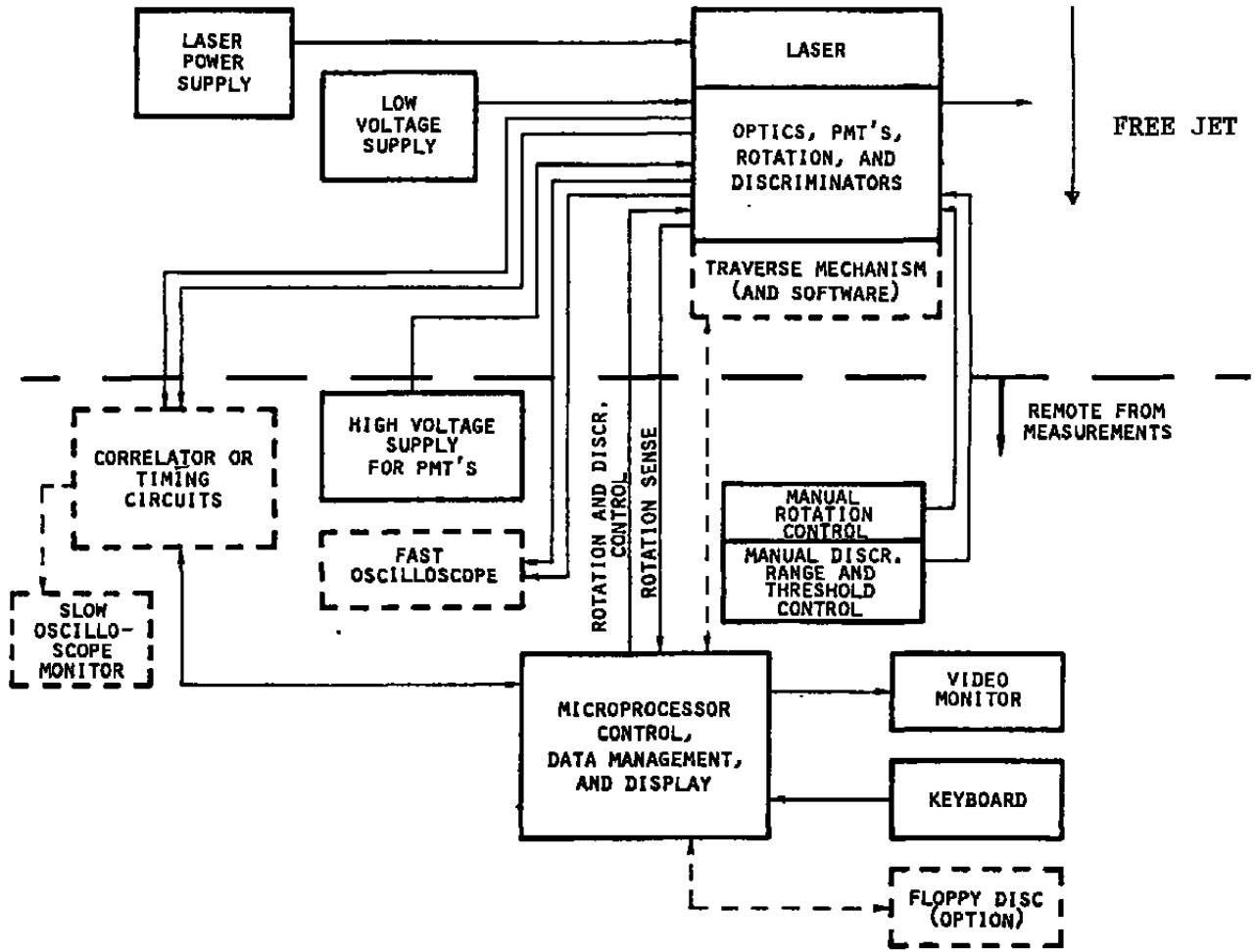

Figure 12. Block Diagram of SDL LTA System.

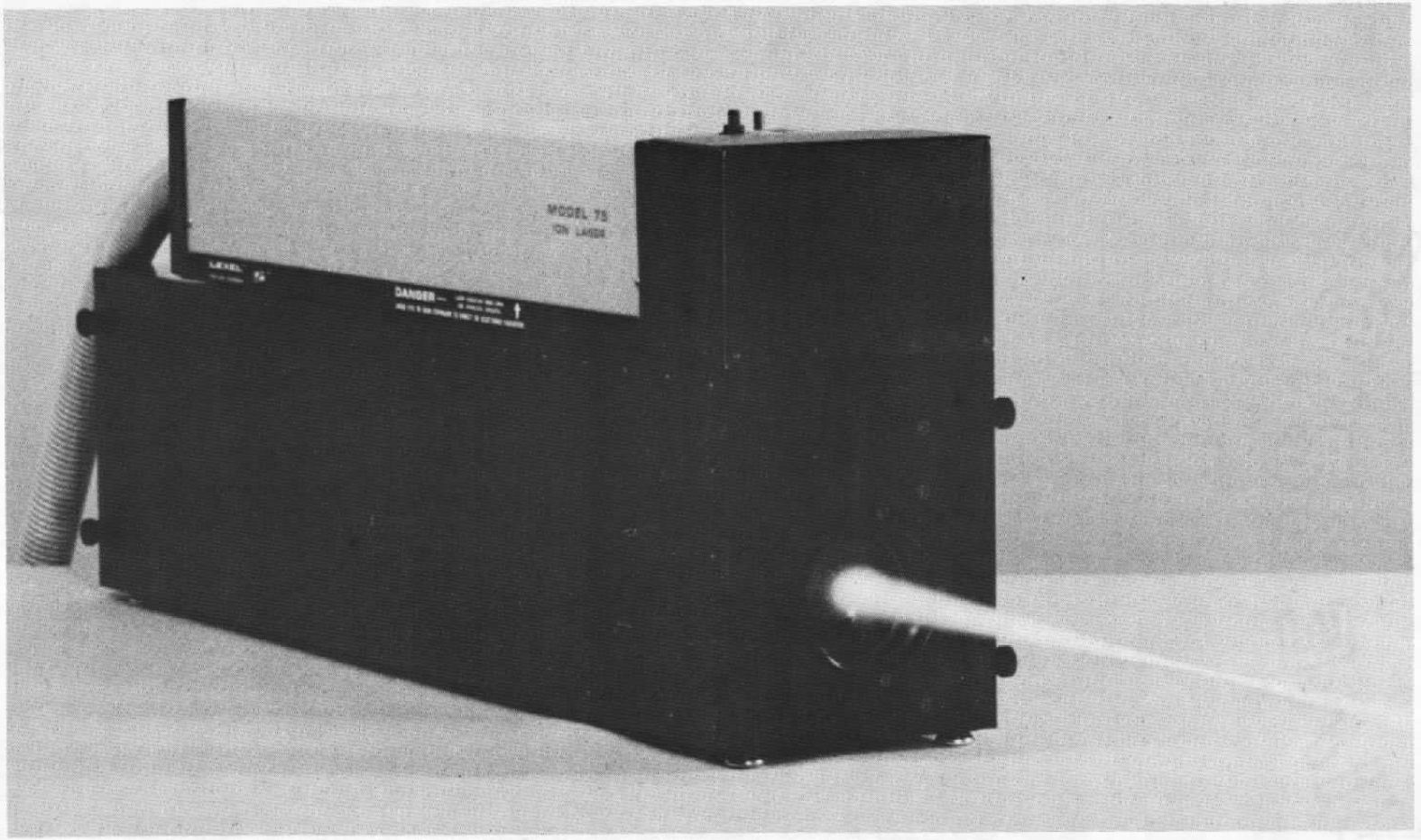

Figure 13. Overview SDL Laser Transit Anemometer (LTA) Optical Head.

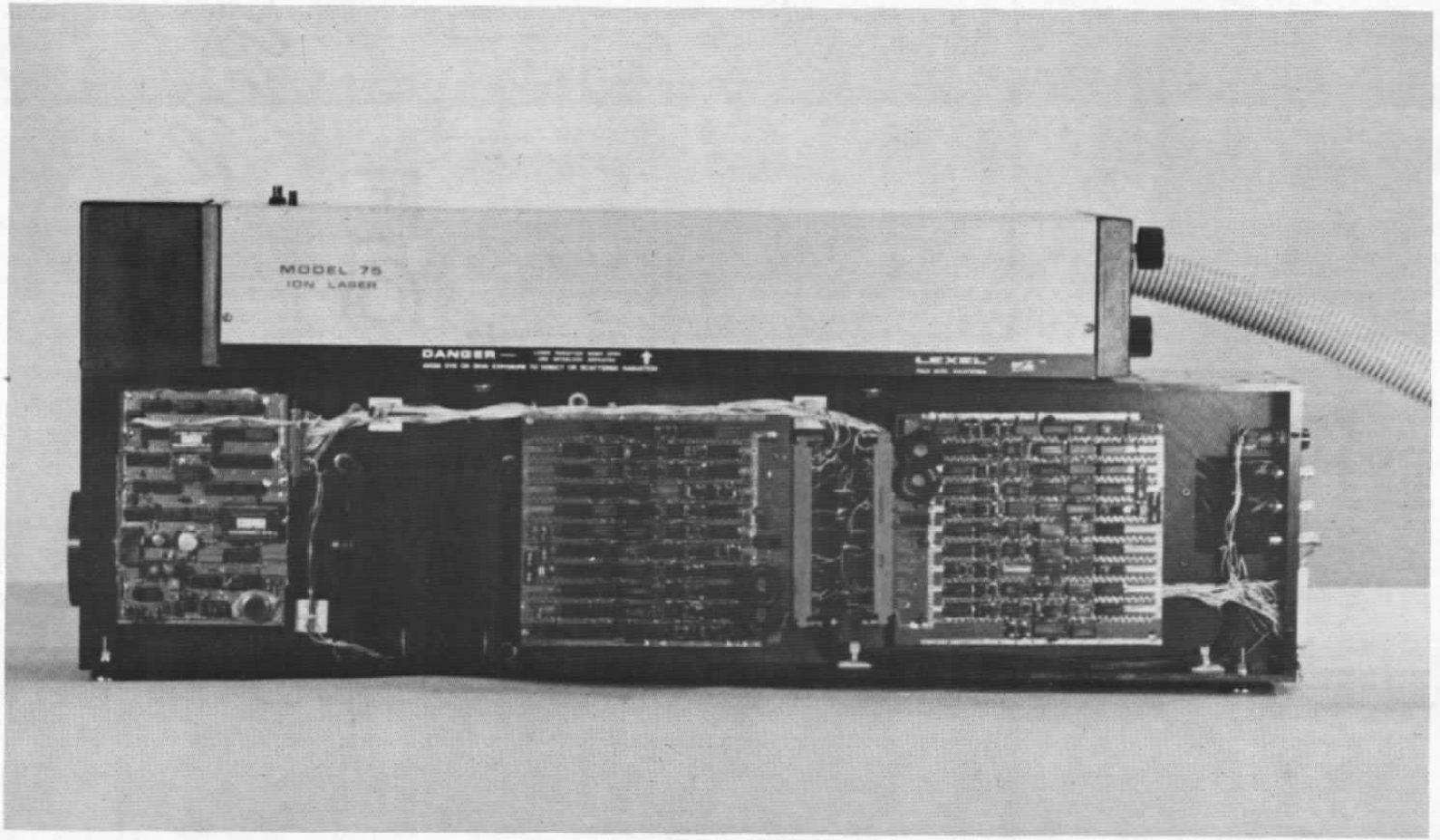

Figure 14. SDL LTA Electronic Components.

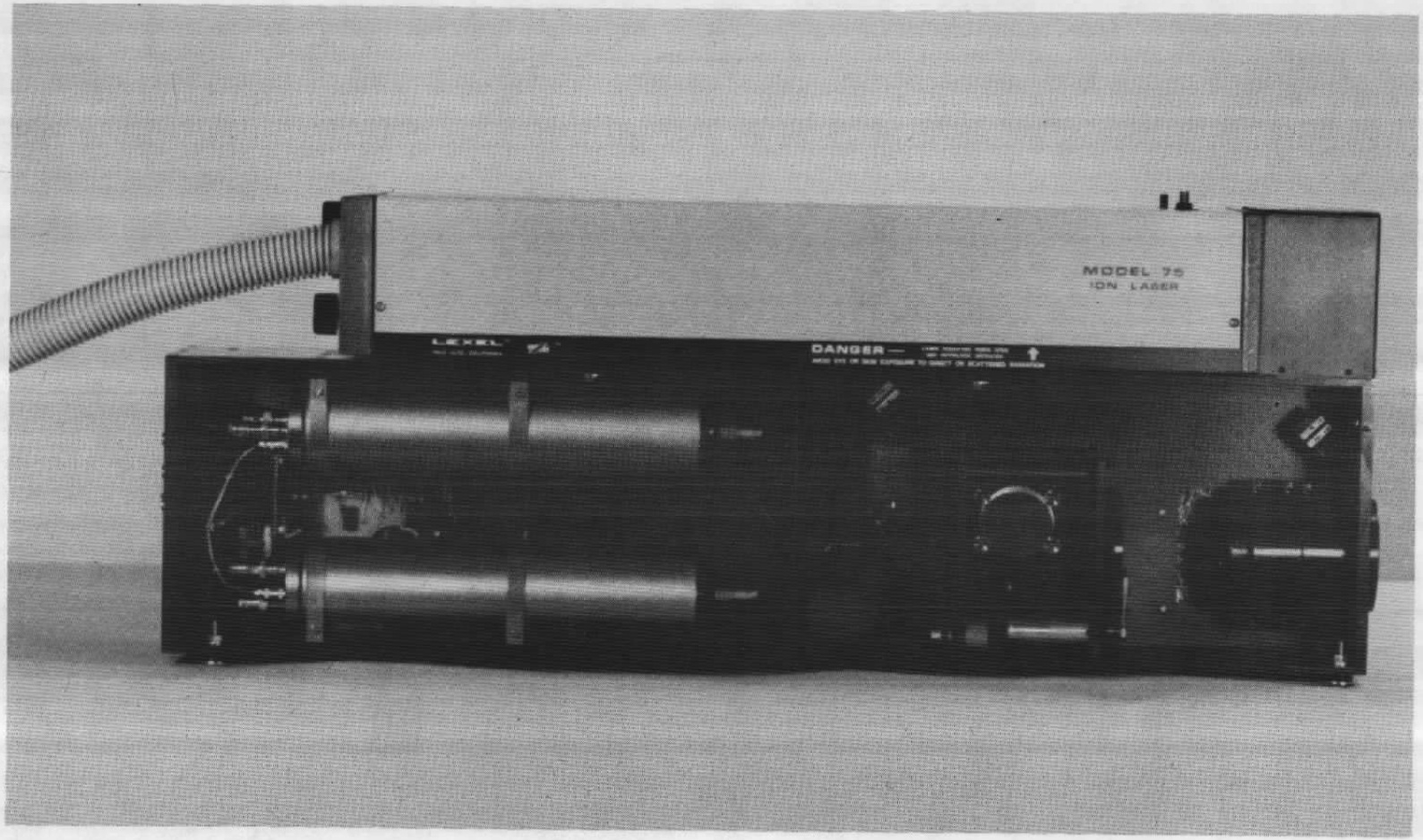

Figure 15. SDL LTA Optical Components.

Table 2. Optical Head Subsystems: Optical/Mechanical.

1. Main Frame Structure
2. Laser
3. Turning Mirrors
4. Beam Splitter Prism and Focusing Objective
5. Transceiver Mirror
6. Rotator Prism Assembly
7. Transceiver Lenses
8. Field Stop Pinholes and Enlarging Lens
9. Fiber Optics Assembly

Table 3. Optical Head Subsystems: Electronic.

1. Photomultiplier Tube Assemblies (2)
2. PMT High Voltage Relay Board
3. Pulse Discriminator Boards (2)
4. Rotator Control and Sense Board
5. Input/Output Connectors and Cables

these functions. For these reasons, the prism rotator control and the discriminator cards and the digital correlator have all been constructed with digital interfaces and we have modified a commercially available microcomputer with interactive graphic capability and included it in the system.

The microprocessor system performs the following operations: records keyed-in system parameters for the experiment; sets the discriminator range; sets the spot rotator angular position; starts the correlator and reads the correlogram upon completion; displays the correlogram for normalization; allows the operator* to move cursor lines on the screen with a manual controller; uses the cursor positions interactively to compute an estimate of mean velocity and turbulence intensity; computes a desirable angular spacing for the rotation sequence which follows; asks permission to go on or go back; automatically sequences the spot rotator prism and operates the correlator in a sequence of measurements at angles uniformly spaced about the initially selected angle; calculates and displays data peak visibility versus angle and determines an estimate of true flow angle via operator interactive graphics**; and records all input and computed data, including the raw correlograms in a memory array for later transfer to cassette tape.*** The microcomputer system has the capability of direct on-line interface with another master computer or computer data link, but this capability was not used in the AEDC tests.

Appendix B is an operational description of the microcomputer software as developed for the September tests.

---

*New versions of the software written after the AEDC experiments have automated these operator functions. The operator now merely gives permission to the computer to continue.

**This function has been automated by curve fit software since the September 1978 experiments.

***Recent improvements include replacement of the cassette tape with a minifloppy disk system which avoids frequent stopping for data transfer.

3.3 OPTICAL SUBSYSTEMS

3.3.1 Main Frame Structure

The subsystems listed in Table 2 comprise the optical subsystems which are briefly described here. First, the mechanical frame of the optical head was designed with highest priorities for compactness and rigidity to avoid mechanical stress and vibration problems in tunnel environments with inclusion of detector and signal conditioning electronics to avoid electromagnetic interference problems. The unit uses an internal spine plate and interlocking top, bottom, end and middle plates to effect a ribbed I-beam-like structure which simultaneously provides strength and rigidity and separate internal compartments which are optically isolated from each other. The side covers employ black fabric dust and light seals, and the structure is black anodized to improve internal optical isolation. The optical head, including the laser, is 93 cm x 36 cm x 20 cm in length, height and width, respectively, and weighs 40 Kg with all subsystems included. The head was designed for compatibility with a Lexel Model 75-0.2 200 mw argon laser as shown in Figures 13-15.

3.3.2 Laser Selection

The laser was selected as an optimization of power, compactness, and reliability. On the basis of small-particle sensitivity as limited by photon ambiguity alone, higher power than 200 mw is sometimes desirable. However, many practical considerations preclude the use of the higher power lasers which are available. These considerations include: physical size, operator safety, degradation of optical components by burning of coatings, evaporation of atmospheric particulates on optical

surfaces, beam phase front deformation and loss of focus by component heating, significant difficulties in overload protection of high-gain photomultiplier detectors, and, of less importance, cost of purchase.

A mechanical design review showed that the laser would be the limiting length component, and that a penalty would be incurred for using the larger model 85 series Lexel or other competitive lasers. Also, sensitivity simulations indicated that the 200 mw laser would be adequate for making transonic measurements with 0.3×10^{-6} m diameter scatterers*. For longer range and for higher velocity measurements, an increase of power up to approximately one watt with the added burden of Class IV laser safety regulations instead of Class III regulations and the longer length of the Model 85 laser, may be justified. However, deposition of vaporized particulates on the optics during tests with the Model 75-0.2 unit verify that the larger laser powers are not desirable when not required.

3.3.3 Turning Mirrors

The system utilizes four 1-inch diameter turning mirrors on two-degrees-of-freedom mounts. These mirrors were chosen for high reflectivity (98%). The purpose of the mirrors is to fold the laser beam path under the laser to the center of the structure, and to allow small translational and angular adjustments required to get the output beam aligned with the mechanically defined optical axis. Figure 16 illustrates the layout of the optical components.

3.3.4 Beam Splitter Prism and Focusing Objective

The beam splitter assembly contains a quartz Wollaston prism and a 10x microscope objective. The Wollaston prism is located with

* As discussed in Section 2.1 above.

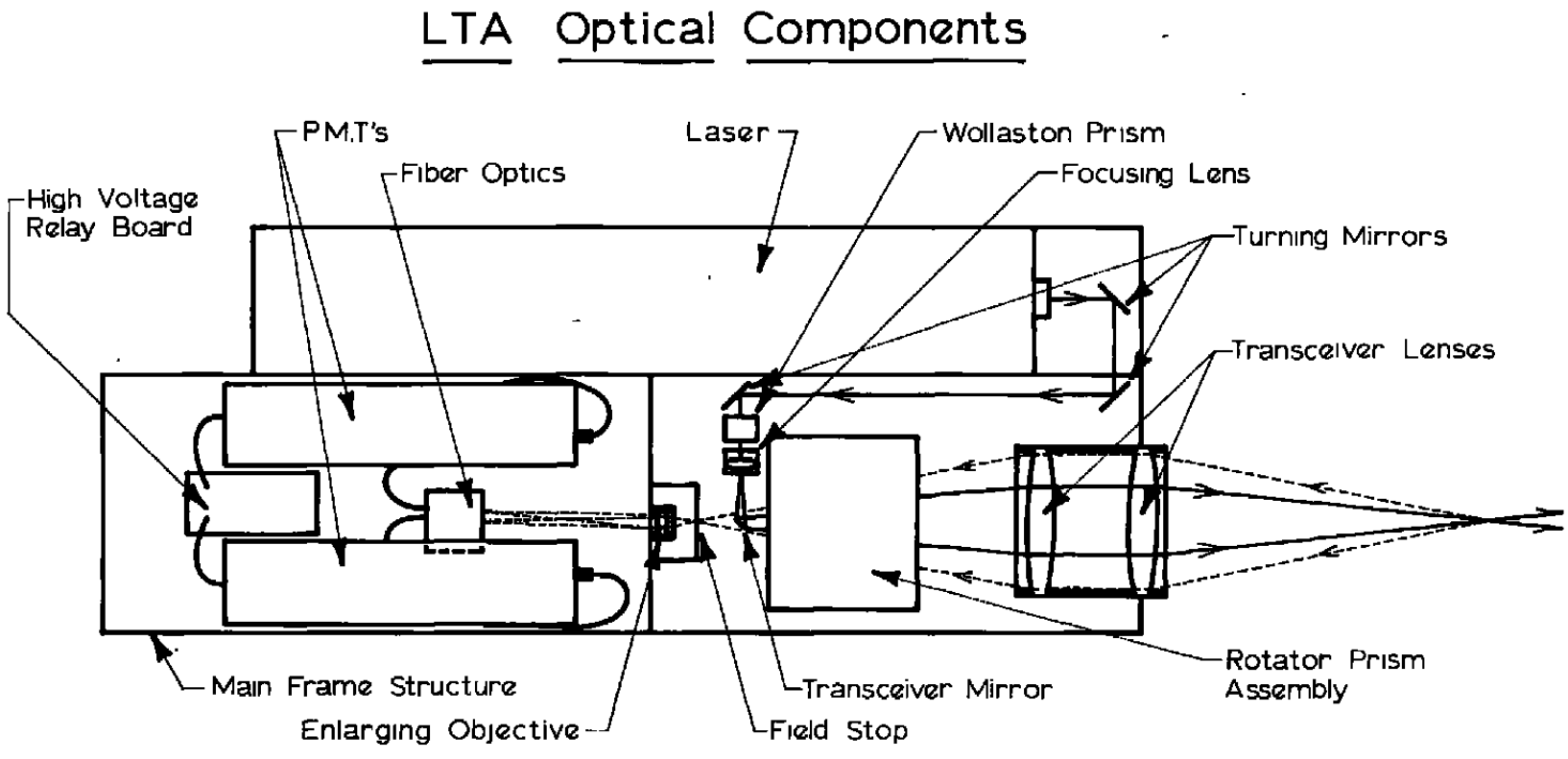

Figure 16. Layout of Optical Components.

its polarization axes at a 45 degree angle with respect to the laser beam polarization. The incident beam is thus split into two beams polarized at 90 degrees with respect to each other, and diverging at approximately one degree. The minimum beam waist diameter is determined from standard Gaussian beam formulas in terms of the input beam diameter incident on the lens, wavelength, and the focal length. The spot separation is determined from the angle between beams and the focal length. The resulting parameters for the experimental system were 12×10^{-6} m diameter ($1/e^2$) spots separated by 300×10^{-6} m; i.e., with a 25:1 spot separation to spot diameter ratio.

3.3.5 Transceiver Mirror

One of the key elements of the LTA optics is the transceiver turning mirror. This mirror follows the generation of the two focused parallel beams and turns them through 90 degrees into the transceiver optical axis. The scattered light which returns from the probe volume to be detected passes around the transceiver mirror which acts as the opaque center stop illustrated schematically in Figure 3 of Appendix A. The mirror was replicated onto a 1/8 inch diameter rod sectioned at a 45 degree angle. The replicated mirror was supported in a spider mount which allows the return scattered radiation from the outer annulus of the receiver to pass around it. High optical quality is required for this mirror because small deviations from flatness will introduce aberrations in the refocusing of the beams in the probe volume.

3.3.6 Rotator Prism Assembly

The rotator prism assembly is one of the outstanding features of the present optical system. In order to appreciate this unique device, one must first realize that the return light scattered back

to the photo detectors should be ideally passed through the center of apertures approximately 20×10^{-6} m in diameter: the diameter obtained by convolution of the transmitted beam focus spot pattern with the diffraction-limited transceiver lens imaging resolution (two-dimensional impulse response). That is, it is desirable for the return radiation to remain fixed in relation to the photodetector apertures to within 1 or 2 micrometers to avoid rotation changes of system sensitivity. If one uses a system which attempts to synchronously rotate the splitter prism and the receiver pinhole apertures, as some have done, then the mechanical difficulties of maintaining alignment during rotation become extreme if not impossible. One solution which has been used by some is to make the pinhole apertures larger; this approach reduces the effectiveness of wall flare rejection. We have taken another approach.

In the previous development of an LTA system, A. E. Smart used a glass image rotating prism through which both the transmitted beams and the return scattered radiation passed. The effect of the image rotating prism on the return radiation is to derotate the image so that it is precisely stationary at the detector pinhole apertures, thus solving the problem of pinhole tracking. Unfortunately, glass prisms of the required size are heavy and, worse yet, produce aberrations of the focusing and imaging system which are intolerable. In previous developments, A. E. Smart used monochromatic light to avoid chromatic aberration and used correction techniques to partially overcome spherical aberration.

The present system utilizes a truncated mirror-dove image rotation prism which consists of a front surfaced mirror and a prism with two external mirror surfaces as illustrated in Figure 17. The design of the prism is such to maximize the angular aperture and thus minimize the internal optical path required while minimizing the weight of the glass. The system is capable of aberration-free operation.

The mechanical assembly which holds and rotates the prism and mirror about the optical axis is illustrated in Figure 18. The same

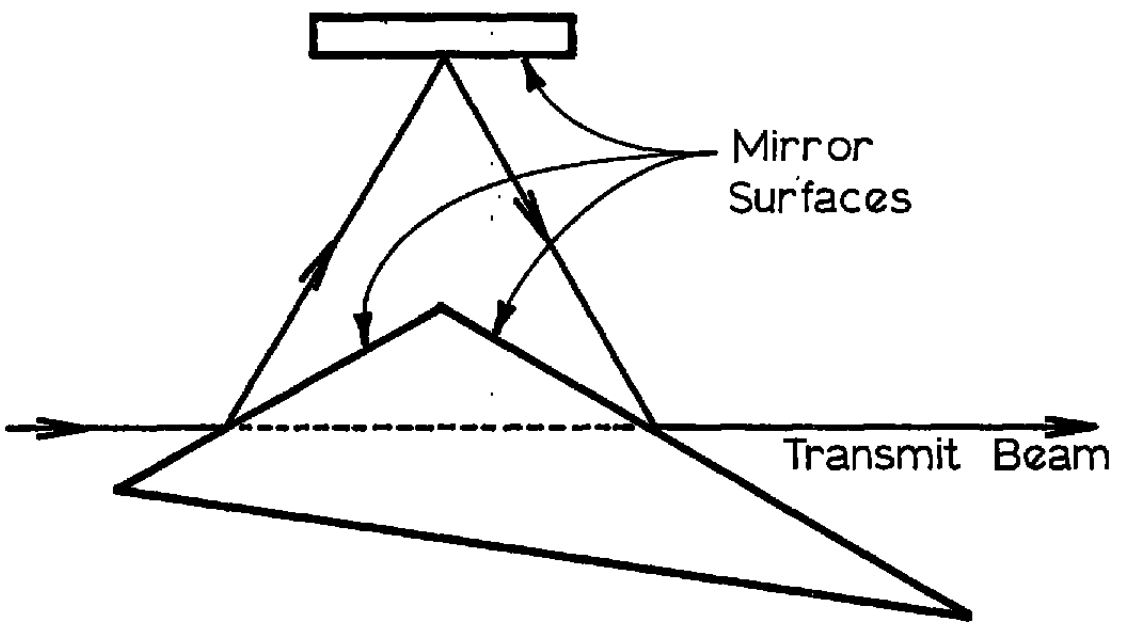

Figure 17. Truncated Mirror Dove Prism.

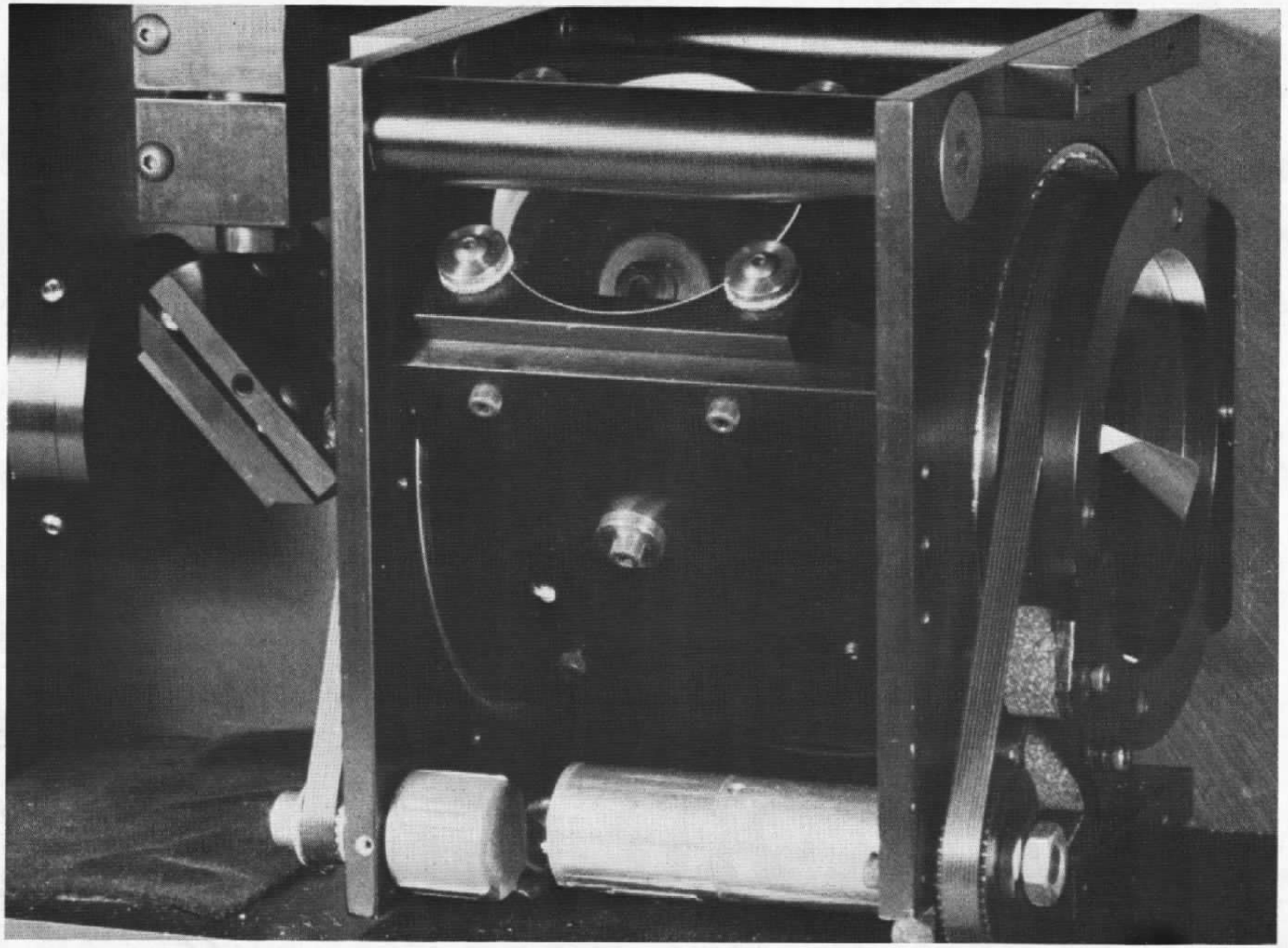

Figure 18. Prism Rotator Assembly.

figure also shows the servo motor gear assembly which drives the prism assembly (lower right) and the linear potentiometer which senses the angular position of the assembly (lower left). The feedback control card, discussed with the electronics later, allows digitally controlled positioning of the rotated image and digital readout of position obtained to 0.1 degree precision. Finally, the figure also shows the mounts for the pinhole apertures (far left), the transceiver mirror (left) and the focusing objective (top left).

3.3.7 Transceiver Lenses

The selection and mounting of the transceiver lenses which image the two focused transmitter beams to the probe volume and the return scattered light back to the detector pinhole apertures is extremely critical. Experience gained with fringe LV systems is very misleading because almost any lens is diffraction limited over the typical small transmitter beam diameters; furthermore, the receiver lens in a fringe system for transonic applications typically must only image light from regions 150 micrometers in diameter or larger. Commonly available telescope objectives easily satisfy the requirements of fringe LV systems without being diffraction limited over their entire aperture, and with minor spherical and chromatic aberrations being unimportant. We now know that such lenses are not always adequate for LTA systems.

In the design of the LTA system for the AEDC, a pair of 80 mm diameter 380 mm focal length cemented achromats was obtained and tested by observing the aberrations in the transmitted focused beams, using multiple wavelength (primarily 514.5 nm and 488 nm) laser operation. The results seemed satisfactory and these lenses were employed in the system. Unfortunately, however, the transmitted beams pass through the central 40 mm diameter portion of the lenses where their performance is the best. Subsequent additional testing of the lenses as receivers

where the scattered radiation is imaged through the outer annulus (radius in the region 20mm $\leq r \leq$ 40 mm) showed that the lenses exhibited spherical aberrations which produced image spots on the order of 100 micrometers in diameter instead of 20 micrometers, and with best focus of the blue (488 nm) and green (514.5 nm) occurring at slightly different locations. The full extent of the difficulties was not realized until it was too late to obtain new lenses before the scheduled test, so the collection efficiency of the fiber optics (discussed below) was very poor. Measurements later after partial improvement was made indicate that the collection efficiency of the fibers was about 5% due to improper lens focus. During later tests conducted at NASA Ames in October, some improvement in collection efficiency was obtained by demagnifying the return spot images prior to incidence on the fiber optics and using a single wave length selector prism. However, this temporary fix does not give back the lost flare rejection capability which demands high resolution imaging. Future systems will employ better lenses.

3.3.8 Field Stop Pinholes and Enlarging Objective

If all the optical elements were perfect and did not scatter or reflect light, then a pair of 20 micrometer diameter pinhole apertures located approximately 300 micrometers apart (precisely conjugate to the actual spot separation) and arranged such that the scattered light from one beam went to one photodetector, and the scattered light from the other beam went to the other aperture, would work well if such a mechanical arrangement could be obtained. Separating the light from the two beams is easy enough if a 50% beamsplitter is used, but then 50% of the power in each beam is wasted; and the mechanical alignment of 20 micrometer diameter apertures poses some inconvenience. In our approach, the field stop pinholes are deliberately made considerably oversized (about 100 micrometers diameter) for ease of mechanical positioning, and are

followed by an enlarging lens and a second field stop which actually limits the receiver field of view (the end of an optical fiber). The pinhole apertures thus only serve to block off-axis internal flare light generated by reflections and scatter inside the transceiver optics compartment, but this is a very useful function.

The enlarging lens is a microscope objective which re-images the return radiation onto the end of the optical fibers. We have used 200 micrometer diameter fibers with a 10x microscope objective planned to obtain the desired match to the 20 micrometer conjugate spot images. The objective was reduced in power to 7x for the test in September*, but further reduction was not possible due to the latitude of adjustment of the fiber optic assembly.

3.3.9 Fiber Optics Assembly

By choosing fiber optics whose core diameter is the desired enlarged field stop size, we have provided both the spatial filtering function and also a means of separating the scattered light from the two parallel focused beams to separate photomultiplier tubes without space limitation. (The two fiber ends must be positioned a few millimeters apart.) The position of each fiber is separately adjustable so that the receiver may be aligned, but the precision of location required is on the order of 20 micrometers instead of 2 micrometers due to the enlargement of the return image prior to the second field stop.

3.4 OPTICAL HEAD SUBSYSTEMS: ELECTRONIC

In order to avoid electromagnetic interference which often arises in experimental environments and to avoid analog waveform distortion over

* To partially compensate for the lens aberration as discussed above.

long cables, several critical electronic subsystems have been located inside the optical head. These subsystems were listed in Table 3 and are described briefly here.

3.4.1 Photomultiplier Tube Assemblies

The limiting length of the laser allowed room for two 12-inch long housings for 2-inch diameter photomultiplier tubes (PMT's). Two-inch diameter tubes are desirable, instead of the more miniaturized tubes which are available, because they typically have better dynode collection efficiency and better single photoelectron pulse height statistics. We chose a new developmental tube, the EMI D305, which is an improved version of the older EMI 9816. Both are high-gain 14 stage tubes with S-20 photocathode material. The S-20 material was chosen over a lower dark count bialkali material because of its greater red response and higher cathode current. The D305 has a higher gain first dynode which improves single photoelectron pulse height statistics. Unfortunately, EMI was unable to supply but one of the two D305 tubes ordered, and that only much later than promised. A 9816 tube was substituted in one channel, as the tubes are interchangeable. Due to lack of time, detailed tests to compare the 9816 and the D305 tubes were not conducted, but both tubes performed quite well.

The PMT housing contains dynode supply voltage divider resistor network and a fast 10x preamplifier with low output impedance for driving a 25 ohm load (a 50Ω coax cable in parallel with a 50Ω terminating resistor). The cathode is overload protected by a high impedance series resistor, and the first dynode voltage is maintained at a fixed 300 volts by Zener diodes. The direct coupled 10x preamp includes a 250Ω input resistor. This gives an effective voltage gain of 5x, with respect to directly driving a 50Ω coax, in addition to the 10x gain of the preamp. The additional gain is not needed in order to

get adequate pulse charge from single photoelectron events under low light level conditions--the phototube itself is quite adequate under such conditions if the high voltage is turned up to about 2500 volts. The purpose of the preamp is to reduce the average anode current which results under high background light level conditions very close to surfaces. With the preamp and 250Ω load, single photon pulses between 0.1 and 1v amplitude are obtained with high voltage of 2000 volts. In practice, 1800 to 1900v is adequate for detection of photon limited signal pulses.

3.4.2 High Voltage Relay Board

A high impedance direct current sense circuit is used to monitor the average current output of the PMT anodes by properly scaling the average value of the output of the direct-coupled preamplifiers. The circuit is an active low-pass filter with an RC time constant of 0.5 second, and a comparator which opens a high voltage relay if the comparator level is exceeded. The comparator level is the properly scaled value of the PMT maximum average anode current. The maximum average anode current rating is a specification which typically can be tolerated for up to 30 seconds, and will not damage the tube appreciably except as it contributes to long-term tube fatigue. We have more than adequately protected the tubes with the 0.5 second time constant, since the effect is integrated, and the relay trips much faster for larger overloads.

The optical head is equipped with an external reset button which glows red when either of the HV relays is opened. Another reset button with light is provided at the remote keyboard control console so that the relays may be reset if an operator or a computer drives the beam focus into a surface during experiments.

3.4.3 Pulse Discriminator Boards

The pulse discriminator boards are important signal-conditioning circuits which produce identical high-level 25 nanosecond smooth pulses for transmission to high-speed timing electronics when a threshold is exceeded and the "best" pulse center is estimated. It would be a simple matter in principle to design these boards if ideal photon correlation could be used. Ideal photon correlation occurs when every single electron emitted from the photocathode is counted in uniformly periodic intervals, and full multibit products are formed and summed. With an ideal PMT and an ideal full correlator, no discriminator function is required, but such is never realized in practice. There are phenomena which we discuss and demonstrate at some length in reference 16 (Sweden, 1978) whereby real pulse pile-up effects, the finite dead time of discriminators, and the single-bit capability of high-speed real-time correlators do not allow the realization of ideal photon correlation in many practical transonic flow situations. A similar situation prevails here. The ideas are simple: if we set the pulse detection threshold to detect single photo electron pulses, then when multiple photon (semi-classical to classical) signals come along, only one discriminator output occurs instead of many due to the finite low-pass filtering effect of either the PMT output circuits, the discriminator dead time, or the correlator input rate. Thus, even if full product multiplication were available, the signal pulse time locations are numerically saturated and cannot respond.

The practical solution to the numerical saturation effects is to raise the discriminator threshold above the mean single-photoelectron pulse level to emphasize statistically the events where finite bandwidth (low-pass filter) effects cause the analog signal to be higher. We have demonstrated experimentally that this course of action does produce a better signal-correlation (peak) to background-photon-correlation

(flat) ratio. And, thus, we see that with existing technology we are forced to admit a semiclassical filter/pulse detection optimization problem where idealized photon correlation is not the solution. Experimentally, we have shown that simple classical assumptions which require large thresholds and zero-background single-photoelectron events are also not optimum: the available number of larger particles is less (and less desirable for particle inertia reasons). We are, therefore, forced to a practical optimum in the "photon limited" regime where signal pulses are the sum of a small number of photoelectron pulses and are only probablistically discriminated against background events. Furthermore, there are two tasks which the discriminators perform: one is the detection of pulses and the other is estimation of the center of a pulse or a group of single photoelectron pulses which arise from a single particle transit. The optimum filters for accomplishing these two functions are different. The pulse center estimation filter requires integration over the classical pulse duration; the time constant of the detection filters must be less in order to avoid biasing the detection towards the slower particles in turbulent flow.

The discriminator boards have seven overlapping ranges whose detection filters have impulse responses which are nearly Gaussian in shape and with pulse widths of 25, 50, 100, 200, 400, 800, 1600 and 3200 nanoseconds. The detection filter ranges are digitally selectable and are labeled range 1 through 7 respectively. Each range also has an integrating pulse center detection filter whose time constant is four times slower than the detection filter for the range. The pulse center detection estimation logic is only enabled logically after the detection threshold comparator is "armed" by a pulse out of the detection filter. The output is then the standardized 25 nanosecond pulse. This approach is more expensive than commonly available constant fraction pulse discriminators which use the same filters for both detection and pulse center estimation. The selection of time constants and the pulse center estimation filter waveforms is such that a given range works without anomalies from the single photoelectron signals up through classical

signals. The discriminator boards also include an isolation amplifier which drives a 50 ohm output signal monitor with the input PMT signal waveform.

A complete statistical analysis of the SDL discriminator circuits would be lengthy and has not yet been undertaken. However, experimental evidence shows that they perform well with photon limited signals.

3.4.4 Rotator Control and Sense Board

The prism rotator assembly is driven by an analog servo motor and gear assembly. An input digital angular address is converted by a D/A converter to an analog voltage. The analog feedback voltage from the linear potentiometer is compared with the requested voltage and the difference integrated and amplified to drive the servo motor. There is a small dead band such that when the desired position is obtained within small tolerances the process ceases. For small angular changes the time constant is approximately 2 seconds regardless of the requested change. For large changes the maximum rate of the motor is reached and the required time may be up to about 4 seconds.

At the completion of an angle change, a flag is set to enable the reading of the linear potentiometer via an A/D converter which is also included.

The servo motor can also be run in either direction, either "slow" or "fast" by use of two toggle switches at the control key where the discriminator threshold level potentiometer is located.

3.4.5 Cables and Connectors

The input connectors for the optical head include the following: A multipin connector for the manual and computer control, and data acquisition system; a multielement connector for the low-voltage power supply; two 50 ohm signal monitor BNC connectors; two 50 ohm discriminator pulse output BNC connectors; two high-voltage BNC inputs for the PMT supplies; and two TTL BNC gate inputs for gating the discriminators.

3.5 OTHER ELECTRONIC SUBSYSTEMS

The total system assembled for the AEDC tests includes electronic power supplies, signal and correlogram oscilloscope monitors, and a 50 nanosecond Malvern correlator as illustrated in the overview schematic shown in Figure 12.

3.5.1 Power Supplies and Oscilloscopes and Manual Control

The signal monitor requires an oscilloscope fast enough and with enough writing intensity to comfortably view pulses of 10 nanoseconds duration. The correlogram monitor oscilloscope can be quite slow. Neither oscilloscope is necessary to the system operation, since the microcomputer data management system displays the accumulated correlograms on the video monitor. However, when the operator is searching for the correct initial angle using the manual rotator control, the oscilloscope monitors provide faster feedback and are thus very desirable.

The system includes a low-voltage supply located physically with the laser power supply, (about 3 meters from the optical head with the present system), and two 2500-volt variable supplies located remotely at the control keyboard. High voltage BNC cable is used to connect these supplies to the optical head.

3.5.2 High Speed Correlator

The system assembled for the AEDC tests included a 50 nanosecond 48 store Malvern correlator. The correlator provides high-speed cross-correlation processing with digital clock accuracy and with only 50 nsec dead time. The theory of the Malvern correlator has been described in detail by Oliver[19] and will not be described here.

SECTION 4.0

EXPERIMENTAL RESULTS

The objective of this contract was to demonstrate an LTA system employing a photon correlator processor and compare the resulting measurements with simultaneously obtained fringe velocimeter measurements. The system described in Section 3.0 was transported to the Arnold Center on September 18, 1978 after a poseponement due to work on the ETF jet facility. Demonstration measurements along the centerline of the jet were made with the LTA system once the facility modifications were completed on Thursday, September 21; however, due to equipment difficulties experienced by the Arnold Center personnel and time and funding constraints which precluded further SDL measurements, no simultaneous measurements were accomplished. In this section we report briefly the results of our experiments.

4.1 ETF JET FACILITY

The tests were conducted using a free jet test installation located in Propulsion Research Cell (R-1A-1) of the Engine Test Facility at the Arnold Engineering Development Center. Assistance was provided to SDL personnel by Mr. T. V. Giel, ETF, Mr. Virgil Cline, PWT, and the facility technicians. A 1" diameter underexpanded unheated jet with a pressure ratio of 4 was used. This jet has been tested extensively in the past with both laser velocimetry and shadowgraph techniques as reported by Barnett and Giel[1] in 1977. Figure 19 is a reproduction of Page 72 of Reference 1 which illustrates the first and second Mach discs located 1.73 inches and 3.39 inches downstream. Due to other activities which had occurred since the calibrations of the jet, a right angle bend had been installed in the jet supply pipe. It is thus possible that minor differences in the flow would occur with respect to the earlier measurements.

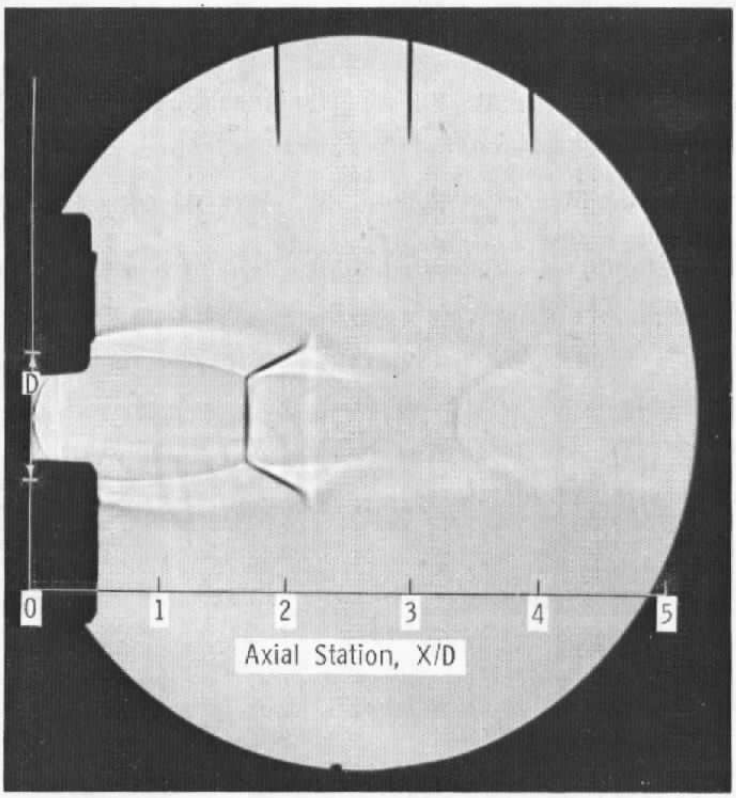

Figure 46. Shadowgraph of underexpanded jet, $P_e/P_\infty = 4$.

Table 4. Mach Disk Locations

	Axial Location, X/D	
Pressure Ratio, P_e/P_∞	Primary Disc	Secondary Disc
2	1.08	2.62
3	1.48	3.05
4	1.73	3.39
5	1.97	3.60

Figure 19. Shadowgraph of Underexpanded Jet, Reproduced from Page 72 AEDC-TR-76-156.

4.2 PRE-TEST ACTIVITIES AND EXPERIMENTAL ARRANGEMENT

The welding modifications to the jet facility were not completed and inspected until the morning of Thursday, September 21, 1978. During the period September 18, 19 and 20, several pre-test activities occurred which are described briefly here.

First, the LTA system was uncrated and the various units interconnected in the control room for checkout purposes. This was accomplished with little difficulty and the system was demonstrated using a small laboratory fan and unseeded room air. The optical system did not need realignment after shipping; however, a few loose connections were discovered in the microcomputer interface which had resulted from improper packing for shipment. These connections were resoldered and the system worked well.

On Tuesday the optical head was transported from the control room to the test cell and the 15 meter cables were installed. Figure 20 is a photograph of the optical head as it was located above the ARO fringe LV system with the probe volumes aligned to be coincident. Figure 21 is a photograph of the data management system with a correlogram displayed on the video monitor.

The optical head was mounted as shown in Figure 19 by removing the side dust covers and bolting it to the support table using the four holes in the base which normally are used for the four feet of the head. After the system was mounted, it was found that the laser had become slightly detuned, apparently due to the change of temperature and physical orientation. Minor realignment of the optical system was required. It was also found that the optical components had become dirty and were producing a lot of internal flare light. The cause for this appears to have been the removal of the side covers immediately after transporting the head from an air-conditioned room to a much warmer and more humid room. The resulting condensation would provide an explanation for the optics getting dirty so quickly, as this had never happened in weeks of previous work with the system.

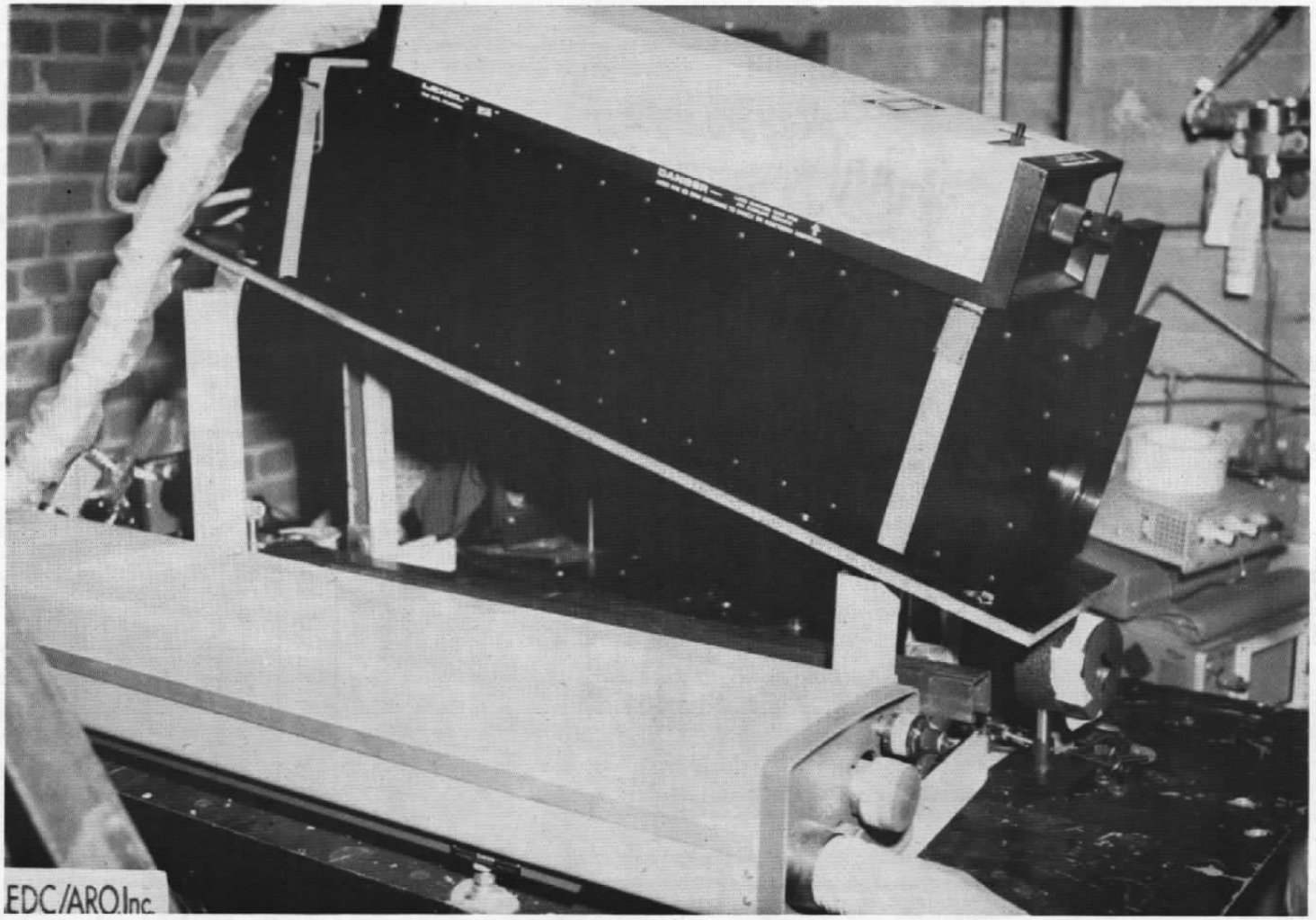

Figure 20. Photograph Showing LTA Optical Head Mounted Above ARO Fringe LV Optics.

Figure 21. Photograph of Data Management System with Correlogram Displayed.

It was also found on Thursday that one of the discriminator ranges was no longer functional. Inspection of the discriminator circuits upon return to Costa Mesa indicated that someone must have inadvertently knocked one of the integrated circuits loose while the electronic side of the instrument was open for mounting of the head, because the discriminator performed normally later when the integrated circuit was replaced.

During the period of time that the LTA system was being set up and checked out, an AEDC fringe velocimeter system was also set up so that simultaneous data could be obtained once the jet facility was operational. On Thursday, the jet was finally operational after lunch, and data taking was initiated. Difficulties with the AEDC equipment caused postponement of the Fringe LV measurements which were repeated the next week after the SDL equipment was shipped back to Costa Mesa on Friday, September 22.

4.3 JET MEASUREMENTS

The output lens used for the jet test was a 622mm focal length lens which resulted in a throw, or range, from the front of the instrument of 597mm, a spot separational 0.489mm as calibrated prior to instrument shipping, and a spot size of approximately 20 micrometers diameter. The axial speed and apparent turbulence intensities as determined by the operator and the data management system were recorded for several locations along the center line of the jet. Photographs were made of the video monitor display which show the choices made by the operator using the interactive graphics approach. All of the photographs of the jet centerline data are reproduced along with the table of raw data in Appendix C. Figure 22 is a plot of the axial speed, in meters per second using the values listed in Appendix C.

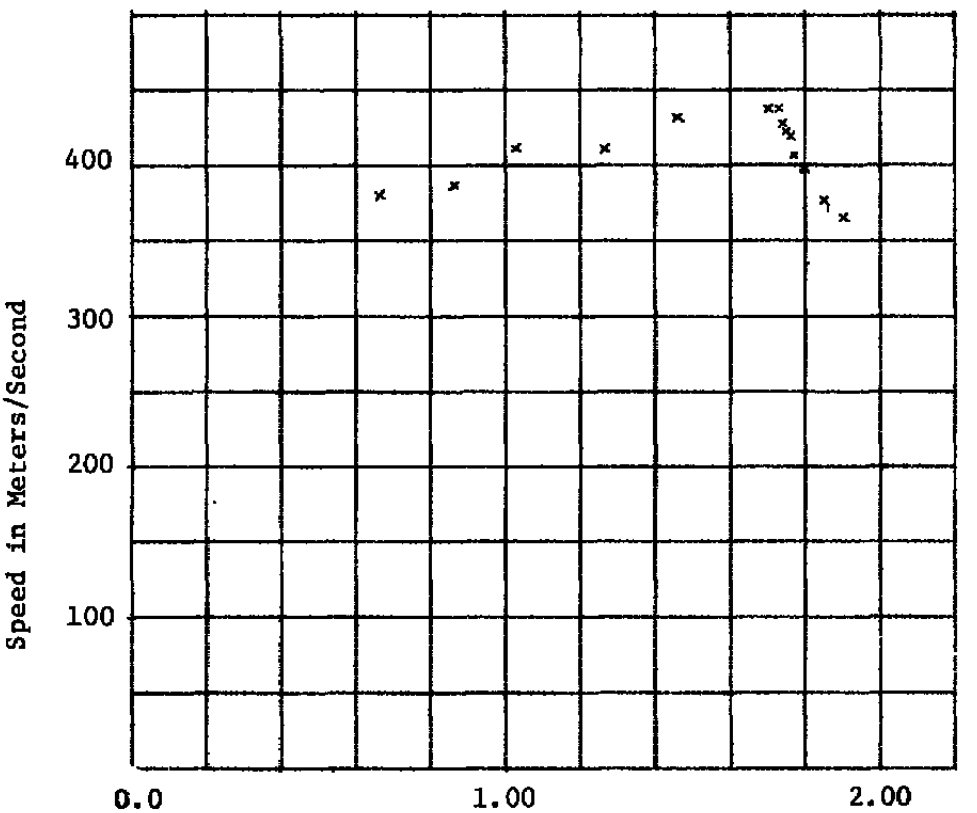

Figure 22. Axial Speed on Jet Centerline.

4.4 DISCUSSION OF EXPERIMENTAL DATA

We are pleased with the relative ease with which data was acquired once the jet was finally available for operation. However, there was insufficient time to make extensive studies of the instrument capabilities. In addition, we learned in later work back in Costa Mesa and at NASA Ames that the system sensitivity was more than an order of magnitude below that of which it is capable.

By hindsight, it would appear that the particles whose velocities were measured must have been nearly one micrometer in diameter or larger. We suspect, in other words, that there were some "boulders" in the jet greater than one micrometer which resulted from the newly completed welds or some other source. Examination of the photographs in Appendix C indicate a distribution of particle lags which produces "apparent" skewed turbulence in regions where little true turbulence would be expected. This effect is partially compensated by selection of the mode velocity in most cases, but we still observe appreciable particle lag effects in the plot of Figure 22; the shock relaxation behind the first Mach disc could have been sharper if the system sensitivity had not suffered from the fiber optic collection efficiency which resulted from the lens aberrations.

At this writing, we have not seen the results of the fringe LV measurements made during the next week. That system used a larger collecting aperture in an off-axis configuration and a 2 watt laser source. There is no way of knowing if the particle size distribution was the same during the fringe LV experiments, so comparisons may be meaningless at any rate.

SECTION 5.0

SUMMARY, CONCLUSIONS AND RECOMMENDATIONS

Spectron Development Laboratories has designed and constructed a physically compact experimental prototype laser transit anemometer system with many innovative features including a microprocessor based data management and control system, an aberration-free digitally controlled spot pair rotation system, a fiber optic detection approach, digitally controlled signal conditioning discriminators, and an automatically controlled interface to a digital correlator.

The system has been transported to the Arnold Center and shown capable of making supersonic backscatter measurements of an unseeded jet flow with co-axial optics and only a 200 milliwatt laser.

In order to make the system more sensitive, easier to clean and align, more reliable, and capable of velocity measurements up to Mach 10, we recommend the following: additional optical system development to include diffraction limited transmitter receiver lens and more easily removable (for cleaning) optical mounts, additional development of the discriminator circuits to include a faster range, and the acquisition of a faster correlation processor. If these steps are taken, a system should result which is capable of measurements up to Mach 10 at ranges of 0.6 to 1.0 meters.

SECTION 6.0

REFERENCES

1. Barnett, D. O. and Giel, T. V., "Laser Velocimeter Measurements in Moderately Heated Jet Flows," AEDC-TR-76-156, April 1977.

2. Johnson, D. A., Bachalo, W. D., and Moddaress, D., "Laser Velocimetry Applied to Transonic and Supersonic Aerodynamics," in AGARD Conference Proceedings No. 193 on Applications of Non-Intrusive Instrumentation in Fluid Flow Research, published September 1976.

3. Mayo, W. T., Jr., "Modeling Laser Velocimeter Signals as Triply Stochastic Poisson Processes," in Proceedings of Minnesota Symposium on Laser Anemometry, held October 22-24, 1975.

4. Mayo, W. T., Jr., "Digital Photon Correlation Data Processing Techniques," AEDC-TR-76-81, July 1976.

5. Thompson, D. H., "A Tracer Particle Fluid Velocity Meter Incorporating a Laser," J. Sci. Inst. (J. Phys. E.) Ser. 2, Vol. 1, 1968, pp. 929-932.

6. Tanner, L. H., "A Particle Timing Laser Velocity Meter," Optics and Laser Technology, June 1973, pp. 108-110.

7. Schodl, R., "On the Extension of the Range of Applicability of LDA by Means of the Laser-Dual-Focus (L-2-F) Technique," Proceedings of the LDA-Symposium Copenhagen, 1975.

8. Cummins, H. Z and Pike, E. R., Photon Correlation Spectroscopy and Laser Velocimetry, Plenum Press, New York, 1977.

9. Mayo, W. T., Jr., "Study of Photon Correlation Techniques for Processing of Laser Velocimeter Signals," NASA CR-2780, February 1977.

10. Abbiss, J. B., Chubb, T. W., and Pike, E. R., "Supersonic Flow Investigations with a Photon Correlator, "Proceedings of the Second International Workshop on Laser Velocimetry, Purdue University, LaFayette, Indiana, March 22-29, 1974.

11. Smart, A. E., "Special Problems of Laser Anemometry in Difficult Applications," AGARD Lecture Series No. 90, 25-26 August 1977.

12. Smart, A. E., "Applications of Digital Correlation to the Measurement of Velocity by Light Scattering," Conference on Laser and Electro-Optical Systems, San Diego, California, 9 February 1978.

13. Smart, A. E., "Data Retrieval in Laser Anemometry by Digital Correlation," Third International Workshop on Laser Velocimetry, Purdue University, LaFayette, Indiana, 11-13 July 1978.

14. Smart, A. E., "Laser Anemometry Close to Walls," Dymamic Flow Conference 1978, Baltimore, Maryland, 18-21 September 1978.

15. Mayo, W. T., Jr., "Ocean Laser Velocimetry Systems: Signal Processing Accuracy by Simulation," Third International Workshop on Laser Velocimetry, Purdue University, LaFayette, Indiana, 11-13 July 1978.

16. Smart, A. E. and Mayo, W. T., Jr., "Applications of Laser Anemometry to High Reynolds Number Flows," Conference on Photon Correlation Techniques in Fluid Mechanics, Stockholm, Sweden, 14-16 June 1978.

17. Mayo, W. T., Jr., "A Two Component LDV System with Photon Counting for the NASA Langley V/STOL Tunnel: Preliminary Design Study," Final Report for NASA Contract NAS1-13737, October 12, 1976.

18. Mayo, W. T., Jr., "Fringe LV Photon Correlation Interpretation Program Software Manual," Final Report for NASA Contract NAS1-14963, 11 November 1977.

19. Oliver, C. J., "Correlation Techniques," in Photon Correlation and Light Beating Spectroscopy, H. F. Cummins and E. R. Pike, eds., NATO Advanced Study Institute Series, Series B; Physics, Volume 3, Plenum Press, New York 1974.

APPENDIX A

LASER ANEMOMETRY CLOSE TO WALLS

Presented at

Dynamic Flow Conference 1978
Baltimore, Maryland
September 18-21, 1978

Dr. Anthony E. Smart
Spectron Development Laboratories, Inc.
3303 Harbor Blvd., Suite G-3
Costa Mesa, California 92626

ABSTRACT

Schodl[1], and others, have reported the development of two-spot or transit anemometer systems. These systems appeared superficially to make unsophisticated 'time of flight' measurements. Work at Rolls-Royce[2] and Spectron Development Laboratories[3] has led to improved second generation optical systems and data processing techniques with significant advantages over fringe laser velocimeter systems in certain applications.

In this paper some advantages of transit anemometry for measuring close to walls and in periodic flows are demonstrated. The unquestioned superiority of this approach for flare rejection does not necessarily lead to longer measurement times. The more complete data gives two-dimensional velocity probabilities and shear stresses in places not easily accessible by standard techniques. Gated measurements are shown for non-stationary situations such as rotating machines and other cases not easy with backscatter fringe anemometry. The high accuracy of the technique is a clear bonus as velocities are easily measured to 0.5% and 30 arc minutes using sub-micron particles. The high dynamic range of this device, 1 ms^{-1} to 1000 ms^{-1}, also increases its usefulness in a number of normally difficult situations.

INTRODUCTION

Conventional real fringe laser anemometry has an impressive history of successful applications where the signal received from small scattering particles is not too seriously swamped by stray light from other sources. In many recent applications, attempts to use fringe anemometry have been frustrated by light scattered at the laser wavelength from machinery close to the sampling volume, for example, walls and blades in turbo-machines.

STRAY LIGHT REJECTION

Light scattered at wavelength other than that of the incident laser may be rejected by suitable filters; and to this end some work has been done on fluorescent mechanisms, either as a fluorescent seed where the wavelength shifted light is accepted or as a fluorescent coating to the wall in question permitting rejection of the scattered light from the wall. The former has been very successful but requires the addition of special seed and the prevention of its deposition on the surfaces which may give troublesome scatter. The latter is not very effective as the mechanism of fluorescent coating is such as to carry the active absorber in a transparent medium. Only the light which enters the medium can be absorbed. That which scatters at the surface is just as troublesome as that scattered from the surface before coating. The unsurprising behavior of some coatings is shown in Figure 1 for 45° laser incidence. The laser used was helium neon and a suitable fluorescent absorber was methylene blue in gelatin--a somewhat fragile coating not suitable for use in hostile conditions. (A carrier other than gelatin could be found.) Figure 2 shows a normally incident beam and the equivalent curves. The key to the letter identification in Figures 1 and 2 is shown in Table 1.

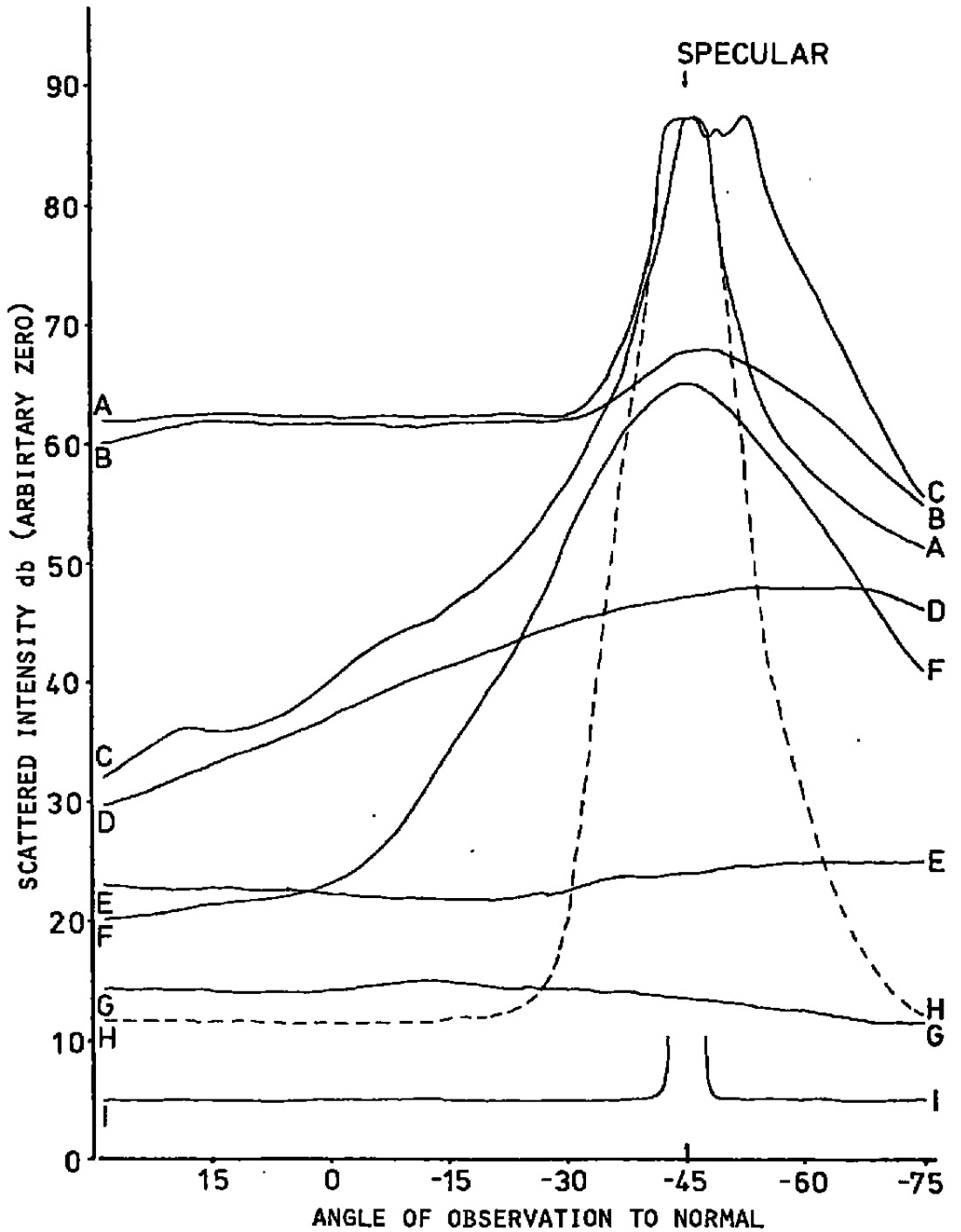

FIGURE 1. LIGHT SCATTERED FOR 45 DEGREE INCIDENCE.

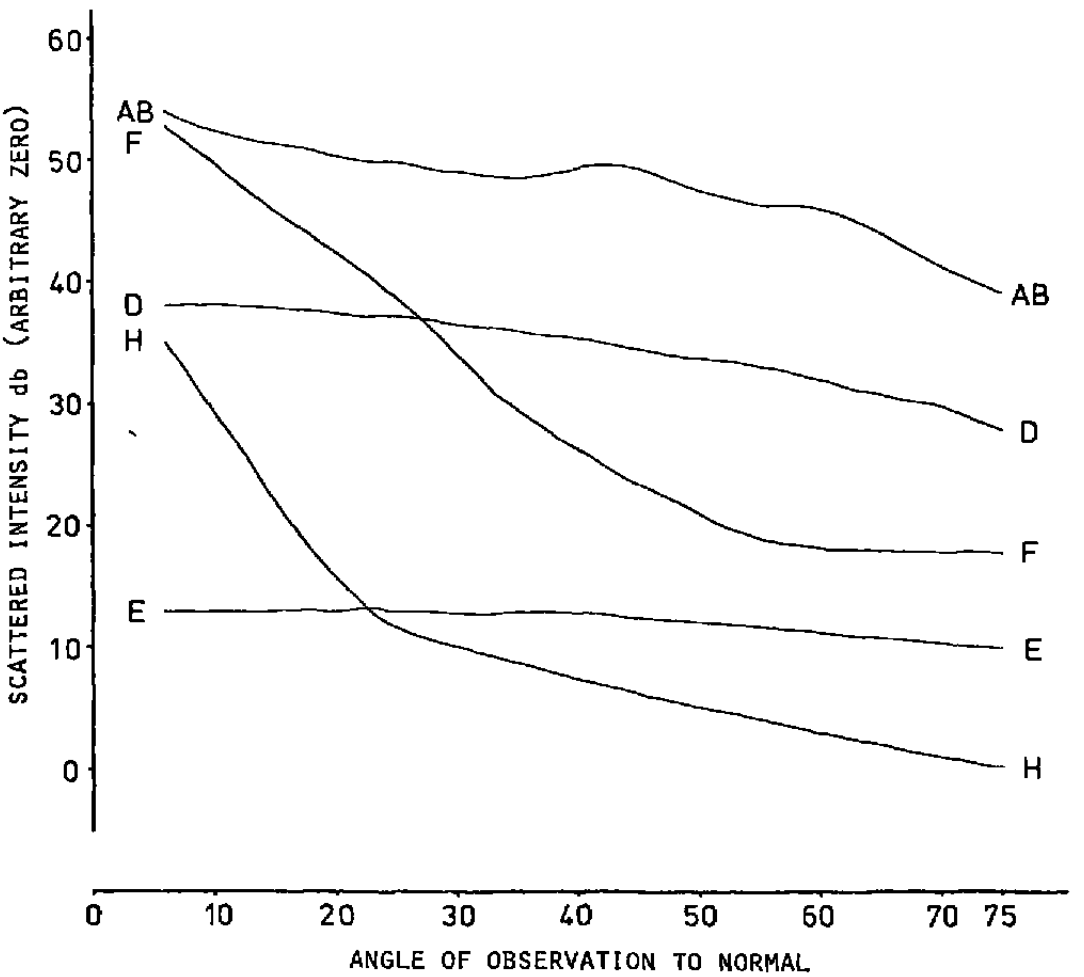

FIGURE 2. LIGHT SCATTERED FOR NORMAL INCIDENCE.

Table 1. Legend for Figures 1 and 2.

A -- Sprayed Matt White Paint

B -- Sprayed Matt White Undercoat (more Lambertian)

C -- Machined Aluminum (milled with some blaze asymmetry)

D -- Brushed Matt Black Paint

E -- Candle Smoked Carbon

F -- Sprayed Matt Black Paint

G -- Black Velvet (delustered rayon)

H -- Sprayed Matt Black Paint with 0.1-0.2 mm Overcoat Layer of Methylene Blue Loaded Gelatin

I -- Clean Optical Glass

It is clear from this that stray light can be reduced by these methods, but they involve modification of the test situation which is, of course, undesirable in many cases.

GEOMETRICAL CONSIDERATIONS

Geometrical subtlety is a superior method of rejecting stray light. The correct devising of optical systems and optimal stops is not trivial. Using fringe systems ways to minimize focal depth, and hence the susceptibility to scattered light from nearby walls, are to use a wide aperture lens or to use oblique observation. The latter is very effective but is not always convenient. It is frequently impossible to accommodate windows so large that they may be used with such a system. Indeed in most situations where wall flare is a problem, there is a constraint to have very small windows. A coaxial backscatter system is a first choice and the use of proper stops to reject wall flare is essential.

Here a transit system has some merit since it concentrates its light into a much smaller volume -- yielding brighter light from scattering particles and reduced light from background. Let us compare two systems, fringe and transit in an attempt to make some quantitative estimates.

Firstly consider the receiving system as comprising the stops shown in Figure 3. The geometrical analysis is very simple. We know that the illumination is the highest on axis and consider the amount of light receivable from axial points -- coordinates x, measured as positive away from the detector.

In consideration of Figure 3 we may look at purely geometrical extreme rays, noting that in a real system there will be very significant effects of diffraction. Diffraction serves to smear the clean lines of Figure 3 but in no way changes its conclusions. We assume that the lens is perfectly corrected for the appropriate conjugates, but this is usually too difficult or too expensive to generate if the system is to be at all versatile. To the extent that this criterion is not met, ultimate performance will be inferior to the geometrical ideal outlined here.

We will use Ω as proportional to the total solid angle indicated by a limiting ray cone and note the formulae of Table 2 in the notation of Table 3.

Table 2. Formulae for Limiting Solid Angles.

Outer Value of Ω.	$\frac{D^2}{(2f+x)^2}$	$\frac{(2f-x)^2}{(2f+x)^2}\frac{a^2}{x^2}$
Valid x Range	$0 < x < \frac{2fa}{D+a}$	$x > \frac{2fa}{D+a}$
Inner Value of Ω.	$\frac{(2f-x)^2 b^2}{(2f+x)^2 (f-x)^2}$	$\frac{(2f-x)^2}{(2f+x)^2}\frac{a^2}{x^2}$
Valid x Range	$0 < x < \frac{af}{b+a}$	$x > \frac{af}{a+b}$

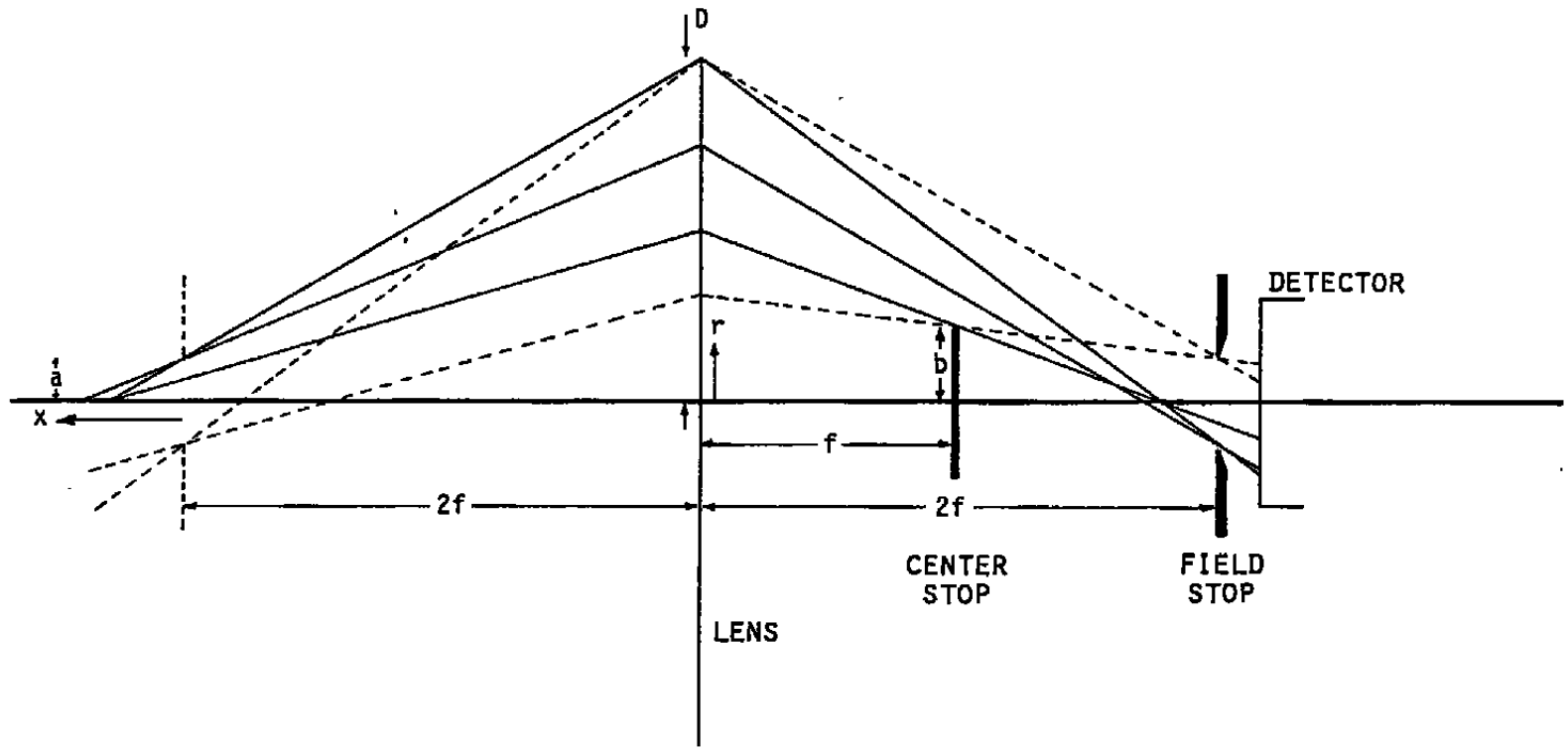

FIGURE 3. SCHEMATIC FOR OPTICAL STOPS.

We may evaluate the expressions in Table 2 for two conditions under which fringe and two spot systems may be comparable.

Table 3. Parameter Specifications

	Symbol	Fringe	Transit
Receiver Aperture Radius	D (mm)	40	40
Sample Volume and Outer Stop Radius	a (μm)	250	10
Receiver Focal Length	f (mm)	250	250
Inner Stop Radius	b (mm)	10	10

Thus, all quantities except the stop size/sampling volume width are identical in both systems.

Figure 4 shows a graph of the normalized intensity which may be collected from a luminous point on the system axis a distance x (m) measured in a direction away from the receiving lens, the direction of interest in the rejection of light from walls. The normalization is performed as though the entire receiver could be used. With the addition of a center stop, to permit the center of the lens to be used for the outgoing beams, the plotted efficiency is reduced from its normalized value. Such a center stop is also that which limits the length of the sampling volume to the extent that we show. For comparable optics it is clear that the improvement in sensitive length is from fringe of 6.1 mm to transit of 0.25 mm. This represents a factor of ~25 which is somewhat degraded both by diffraction and residual lens aberrations but is still a very significant improvement. With a small change in optical arrangement for transit systems, the receiver center stop may be made larger than we have shown. The reduction in overall

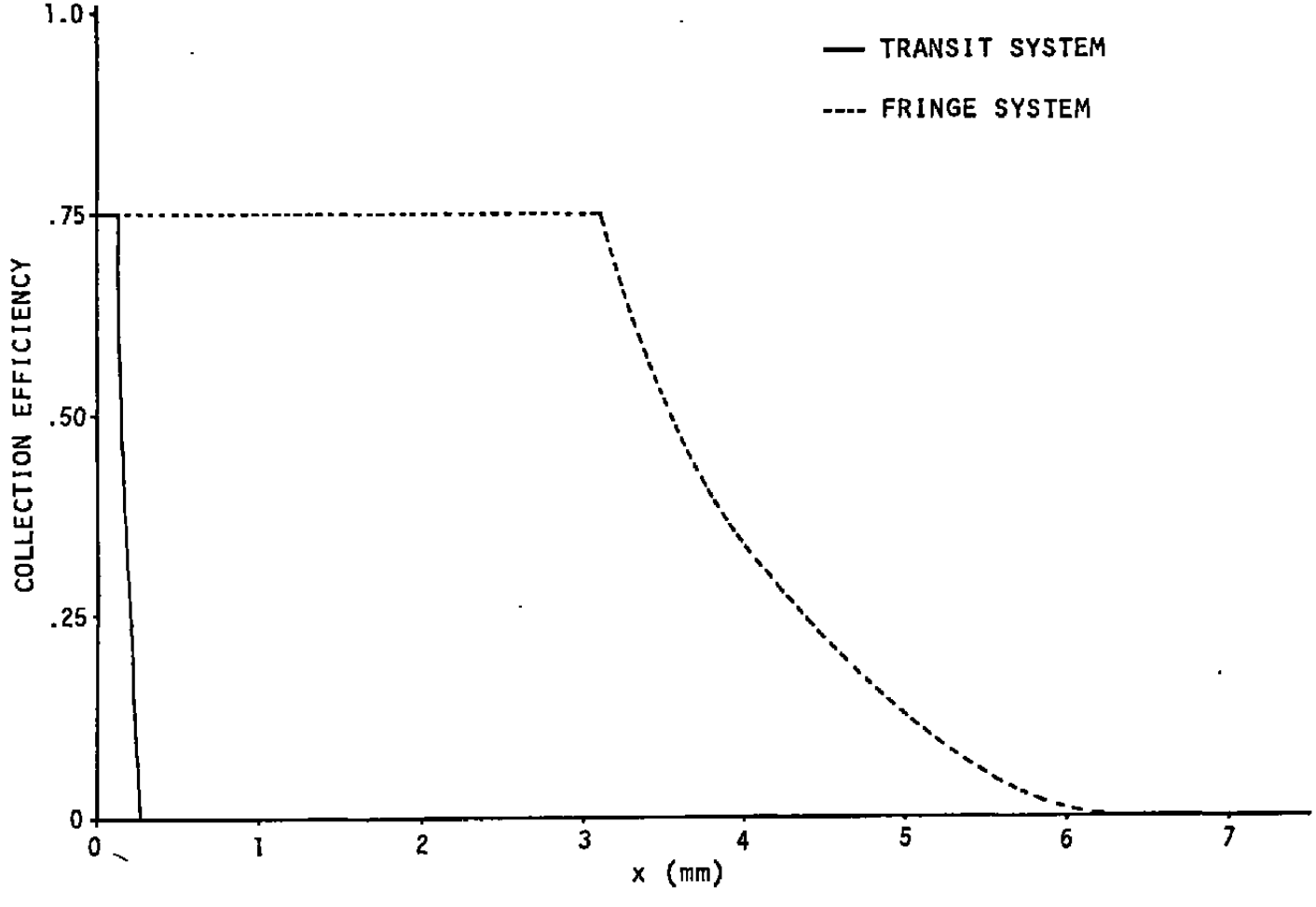

FIGURE 4. AXIAL COLLECTION EFFICIENCY OUTWARD FROM RECEIVER (FROM FIELD STOP IMAGE).

efficiency is then a tradeoff with the reduced sensitive volume length, which may thus be shortened even further.

The quoted collection efficiencies must be taken in conjunction with where the incident light is available to be collected and represent a further increase in the roll-off rate shown. This is simply a factor of $\sim x^{-2}$ for the transit system and $e^{-y^2/2\sigma^2}$ for the fringe system; y/σ is a beam parameter near the waist of the fringe generating beams. Substituting values appropriate to the former example, the 1/e point of illumination intensity along the axis is about 480 μm for the transit system and 17 mm for the fringe system. (This corresponds to forty 12.5 μm fringes.) In both cases it is seen to be the receiver aperture which is the critical component.

We have only considered axial properties and it is clear that there will also be contribution to unwanted flare from off-axis positions which receive illumination. The contours of constant flare will be represented by the lines of constant product of the illuminating and receiving hyperboloids, with allowance for the near paraboloidal truncation on axis. This will reduce the efficiency of both systems to a comparable extent since we have supposed that the transit system has been illuminated by a cone not far separated from the inner boundary of the receiving cone, and also that the fringe system is illuminated by beams close to the inner receiver cone boundary but with reduced divergence. It is apparent that these constraints are more serious on the receiver side of the focus which we have not considered here as they do not have a significant effect on wall flare. An analogous analysis could be performed for the receiver side of the sampling volume. This would have relevance to dirty windows. The specular window component must, of course, be rejected by obliquity. In flows with many particles there is some possibility that this effect could limit the maximum tolerable particle concentration.

OTHER ADVANTAGES

For the geometries we have considered, the increase in illumination intensity at the sampling volume is somewhat under a factor of 200 when going from the fringe system to the transit system. Because this makes possible the acquisition of good signals from smaller particles, the data rate need not fall by a similar factor in a naturally seeded system which may contain more smaller particles.

The observation of a velocity probability in a chosen direction with facility to rotate the spots about an equivalent centroid makes the measurement of shear stress very straightforward. Also because of the small size and large separation of the spots, typically a ratio of 1:25; the measurements of velocity magnitude and direction can both be very accurate.

The system may have the spot rotation arranged without difficult optical alignment by making the output and received images conjugate. It is highly desirable to do this to take full advantage of the foregoing discussion and arrange optimally small stops. For the SDL transit system we accomplish image rotation by use of a mirror Dove of novel design which works at f/4 or a little better without intermediate image and is aberration free in a diverging beam. This makes the whole instrument quite short. One point of interest is the necessity to reject not only scattered light from each beam into its own receiver but from each beam into the other receiver. This is essential, and of course we use two receivers and further stops designed with the above criteria borne in mind. At each point in the optical design the nature and type of stop should be considered -- whether field, aperture or hybrid.

SOME EXAMPLES

Figure 5 shows the approach to a wall with the earlier Rolls Royce system, and Figure 6 shows measurement in a subsonic fan. Both figures are only illustrations of system performance which has been substantially improved in the newer SDL equipment.

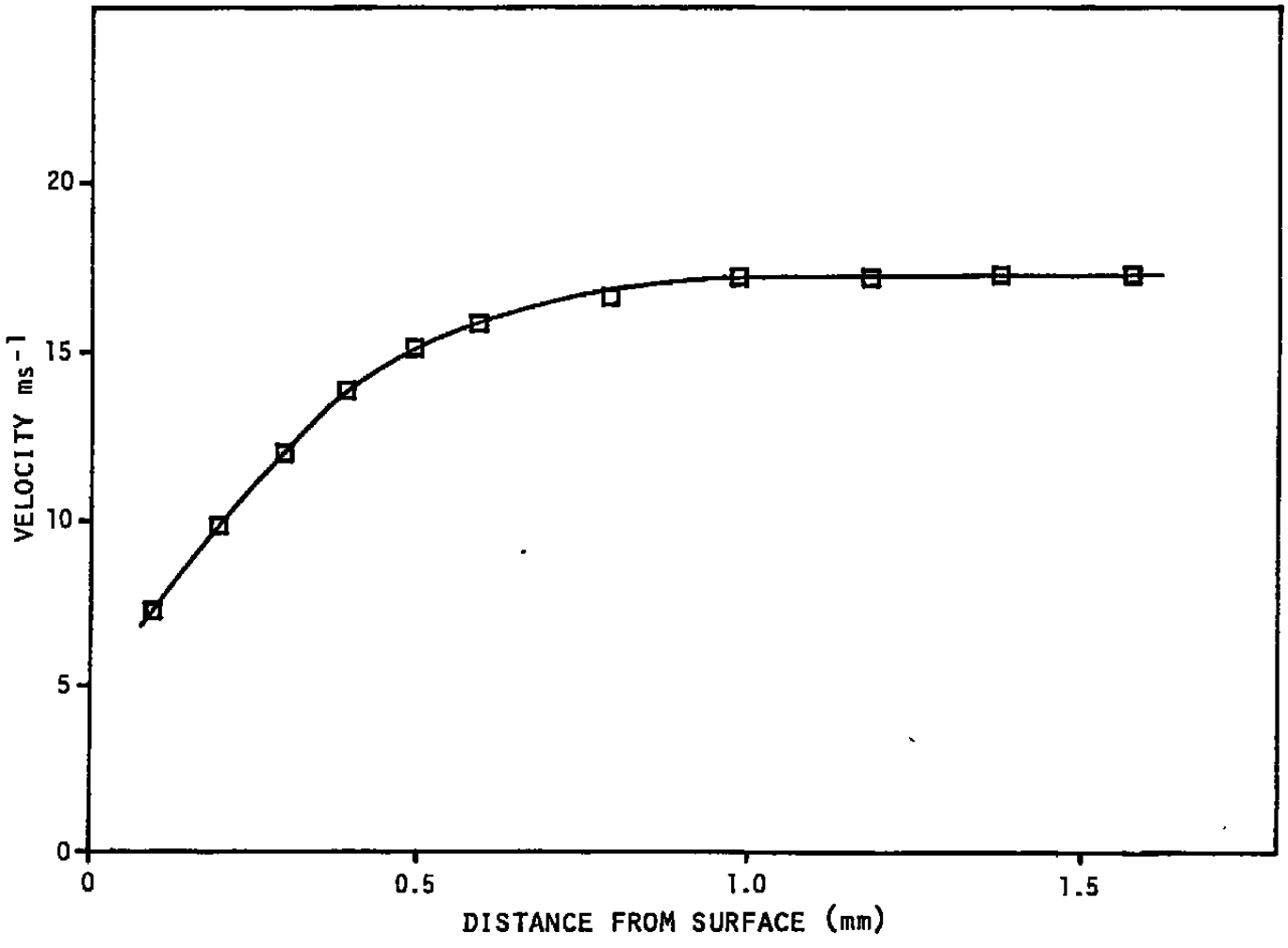

FIGURE 5. BOUNDARY LAYER TRAVERSE ON PRESSURE OF A TURBINE CASCADE.

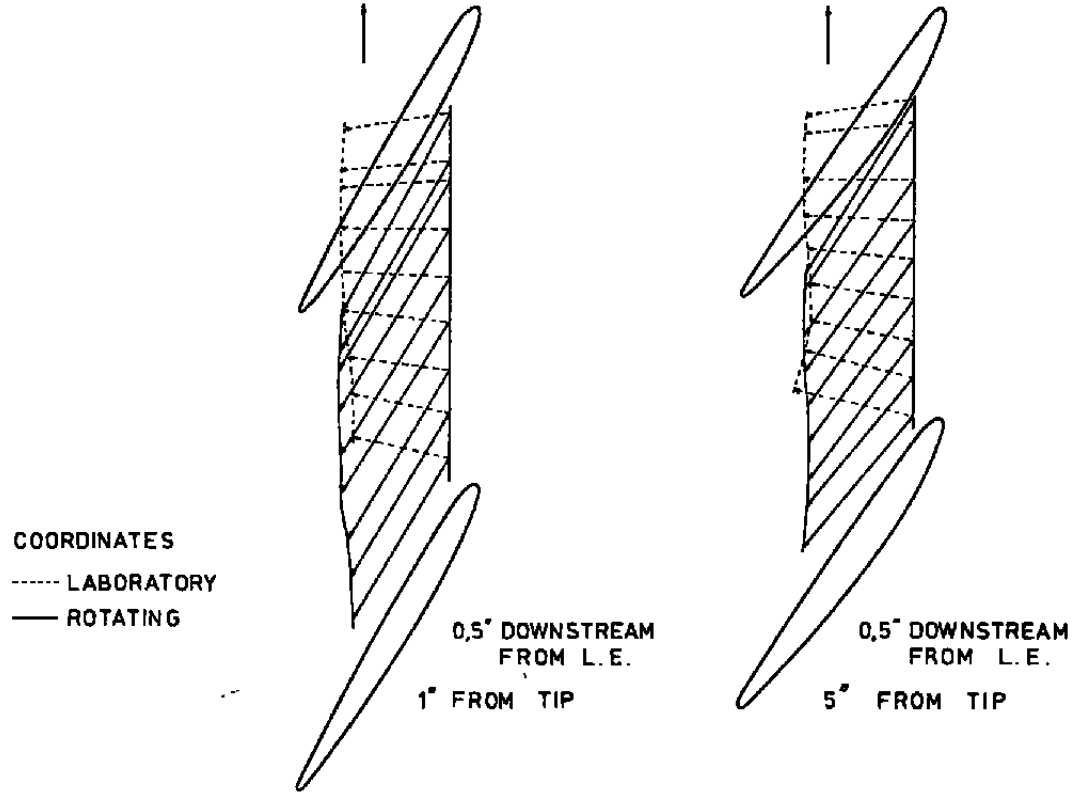

FIGURE 6. INTER-BLADE TRAVERSES AT DESIGN.

CONCLUSIONS

1. Flare light can be most satisfactorily rejected by well considered geometrical design and attention to optical components.

2. The transit configuration allows at least an order of magnitude improvement in the proximity to walls at which good measurements may be made, given similar constraints.

3. The capabilities of the transit system to look at smaller particles and measure stresses by spot rotation are especially useful close to walls.

REFERENCES

1. Schodl, R., "A Laser Beam Method for Flow Measurements in Turbomachines," ASME Paper 74-GT-157, 1975.

2. Smart, A. E., "Special Problems of Laser Anemometry in Difficult Applications," Lecture 6 in AGARD LS 90, 1977.

3. Smart, A. E., "Applications of Digital Correlation to the Measurement of Velocity by Light Scattering," Paper ThHH1, CLEOS '78, San Diego, California, February 1978.

APPENDIX B

OPERATIONAL DESCRIPTION OF MICROPROCESSOR SYSTEM

After the program has been loaded from the tape

*ØG↵	Underline indicates user-typed command or response. "↵" represents hitting carriage return.
RUN↵	
[the screen will clear]	
DATE(MO,DAY)= 9,28↵	Enter MONTH,DAY of today's date
TIME(HR,MIN)=14,3Ø↵	Enter HOUR,MINUTE of this run--use military time, e.g. this example would indicate 2:30 p.m.
SPOT SEPAR.(MM)=	Enter spot separation in millimeters
X,Y,Z=	Enter X,Y, and Z values separated by commas.
DELAY=	Enter time delay in microseconds.
DESIRED RANGE=	Enter desired discriminator range 1-7
THETA SET?	Set rotator angle manually if desired and then hit return
THETA= 9Ø.4	Reports current rotator position
DESIRED THETA= 96.2↵	Enter desired rotator position
THETA=96.2	Reports new rotator position.
GO ON?↵	Hit return when ready to continue.

At this point, the Malvern correlator is automatically started. When the set number of samples has been collected, the Malvern stops (red light goes on) and the plot of the correlogram is drawn on to the terminal screen. Using the "paddle", the user sets certain vertical and horizontal lines on the screen as described on the following page.

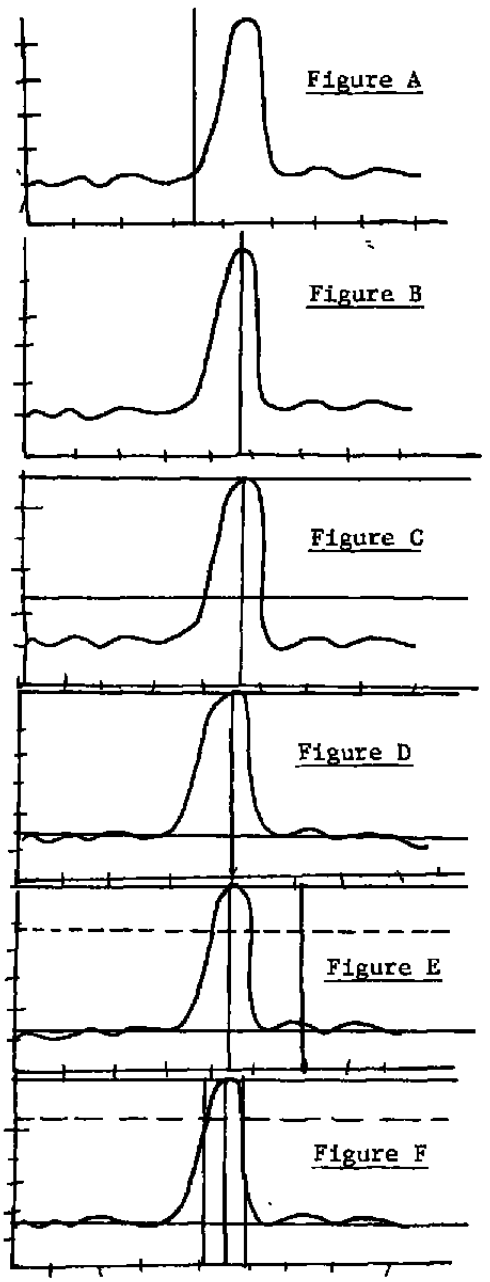

When the correlator stops, a plot such as the one shown in Figure A appears on the screen. The rightmost vertical line can be moved by turning the dial on the paddle. This line should be used to locate the approximate peak of the plot as shown in Fig. B. When the desired position is located, press the button on the paddle to lock in this value and to continue the program.

NOTE Moving the horizontal and vertical lines causes erasing of the function at intersection points. Type any character to have the function replotted.

A horizontal line should now appear along the top of the plot and another horizontal line is available for the user to move (with the paddle). This line should be used to locate the approximate base line of the function as shown in Fig. D. Press the button when the desired position has been reached.

The program now automatically draws a line which is 1/e distance from the upper line. Also another vertical line appears, as shown in Fig. E.

Move this line to one of the points where the 1/e line intersects the function, and then press the button. Another vertical line should then be moved to the other point at which the 1/e line intersects the function, then press the button again. See Fig. F.

The screen clears and then presents the input variables and calculated values in the following format:

DTHETA=	T-ACT=	T-REQ=
V=	TI=	N=
SS=	DISC=	IDEAL=
X=	Y=	Z=

DTHETA - the change in the rotator angle for each iteration (in degrees)
T-ACT - the actual position of the rotator (degrees)
T-REQ - the requested position of the rotator (degrees)
V - the calculated velocity
TI - the calculated turbulence intensity
N - the desired number of angles (DTHETAs) to process
SS - the spot separation (millimeters)
DISC - the current value of the discriminator range
IDEAL - the calculated ideal discriminator range
X,Y,Z - current scan coordinates

DTHETA will remain blank until the value for N (the no. of angles) is specified, at which time the value for DTHETA will be printed out. On the first run, N will remain blank since it will not have been assigned a value yet. After N gets assigned a value, this value will be printed.

The computer next asks:

SAVE THIS RUN? Y↵ — User examines the calculated results to determine if this data should be saved. Hit return if you don't want to save it; type any other character and then hit return if you do want to save it.

If this run is not saved, control passes to start point A. (See page 2)
If this run is saved, then the following options are presented:

If this was not the first run, then:

CHANGE NO. OF ANGLES? Y↵ — Hit return if same no. of angles is desired; hit any other character and then return to set a new no. of angles.

If this was the first run, or some character was entered in response to the question "CHANGE NO. OF ANGLES?", then:

NO. OF ANGLES= 3↵ — After this value is entered, the header information for DTHETA and N will automatically be updated.

GO ON?↵ — Hit return when ready to go on and vary the rotation angle by the calculated DTHETA degrees.

Now, as the rotator alternates in direction from +DΘ to -DΘ to +2DΘ to -2DΘ, etc. until the specified number of angles has been reached,

the program will present plots with horizontal lines on them as shown in Fig. G. The upper line is fixed; move the lower line to the base line of the function and press the button to go on.

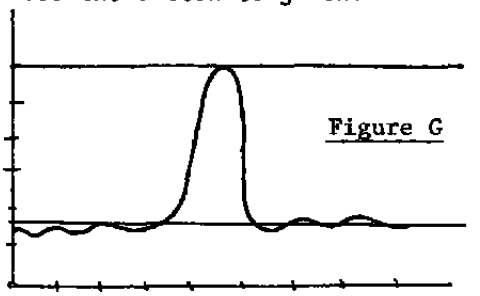

Figure G

When all the angles have been processed, a plot of the visibility ratio at each of these angles is displayed with a vertical line which should be positioned at the estimated peak of the function which would join these points. (See Fig. H). Then press the button.

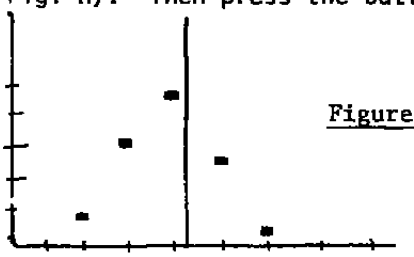

Figure H

The computer responds with:

SAVE THIS RUN?↵ — Hit return if you don't want it saved; type any other character and hit return to save it.

Control then passes to the A start point which continues with the following questions:

This point can be returned to (after aborting the program with RESET) by typing ØG, return, and then GOTO346.

CHANGE X?↵ — Hit return if you want same value of X; otherwise type any character and return.

CHANGE Y? Y↵
Y=2↵ — Enter new value.

CHANGE DELAY?↵

Now the program continues as described previously by requesting desired range, desired theta, etc.

APPENDIX C

RAW DATA

Table C1 is a reproduction of the raw data obtained from the jet centerline measurements. The speed and turbulence intensity are those computed by the data management system based on the operator selection of the vertical censor locations. Photographs were made of the video monitor display for axial locations x/D = 1.06 through 1.90. These photographs are numbered 1 through 11 and are reproduced here as Figures C1 through C11.

Table C1. Table of Results.

Run No.	Photo No.	Time C.T.	Position x/D	Speed MS-1	Turb. %	Tube Volts V	Time/	Threshold
1		14.10	0.66	367.1	15.8	1900	50	3.8
2		14.32	0.66	357.5	16.9	1800	50	4.5
3		14.46	0.66	380.8	18.1	"	"	"
4		14.51	0.86	388.1	15.8	"	"	"
5	1	14.58	1.06	411.6	17.3	2000	50	5.8
6	2	15.05	1.26	411.6	14.6	"	"	"
7	3	15.15	1.46	433.5	15.2	"	"	"
8	4	15.23	1.70	438.2	11.7	"	"	"
9	5	15.37	1.73	438.2	5.6			
10	6	15.41	1.74	428.9	5.95			
11		15.44	1.75	424.5	5.90			
12	7	15.45	1.76	420.1	4.30			
13	8	15.54	1.77	407.5	4.58			
14	9	15.57	1.80	399.5	4.1			
15	10	16.00	1.85	377.3	2.15			
16	11	16.02	1.90	367.1	3.56			

NOTE: Runs 1 through 4 were made before the jet was "on condition" at pressure ratio of 4.0.

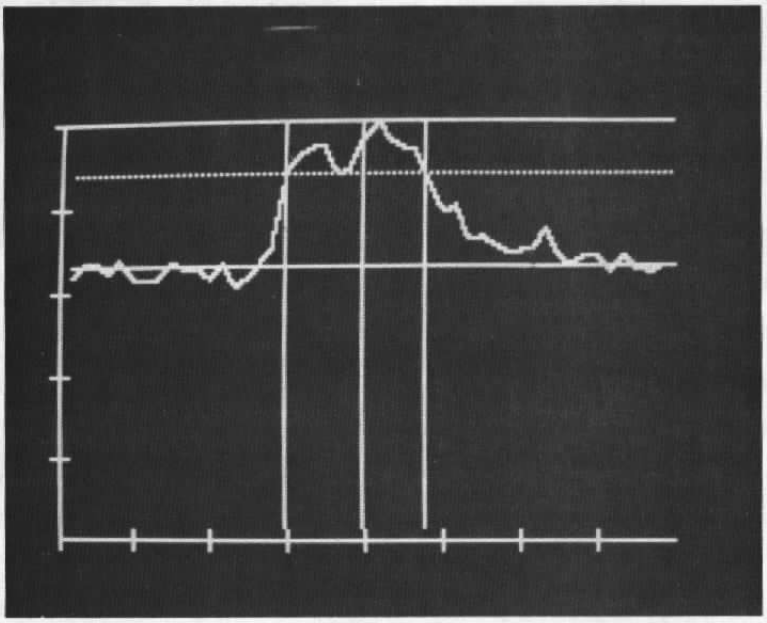

Figure C1.

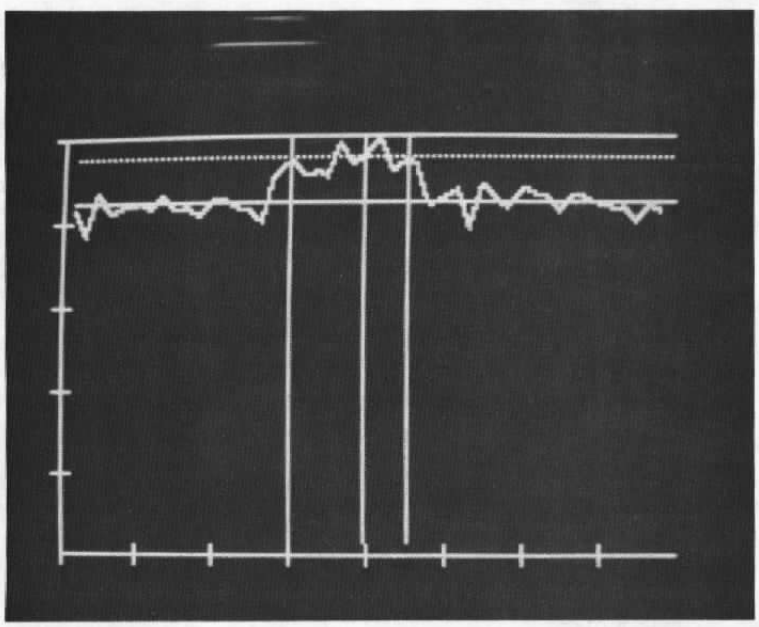

Figure C2.

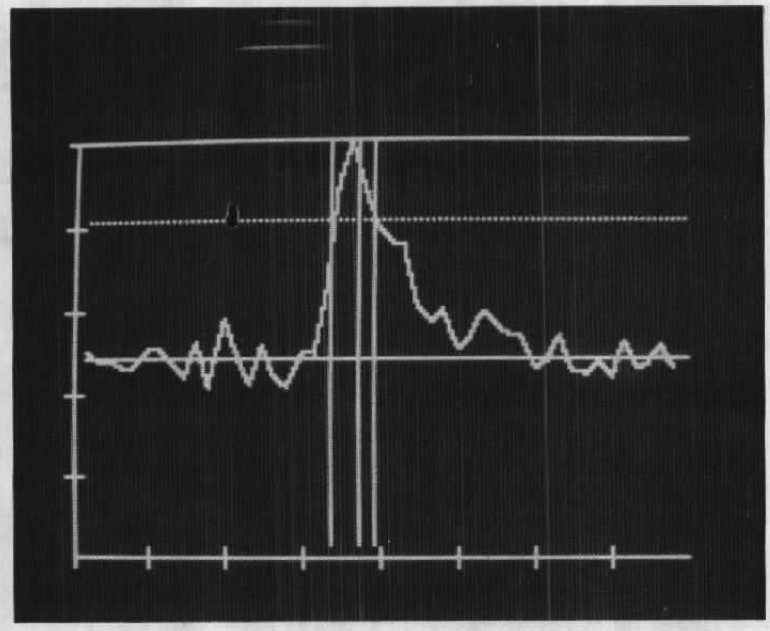

Figure C5.

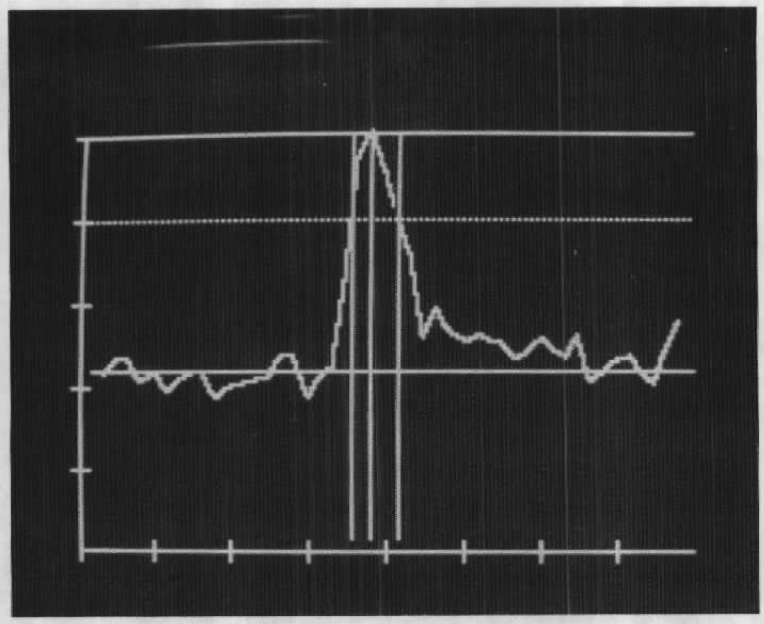

Figure C6.

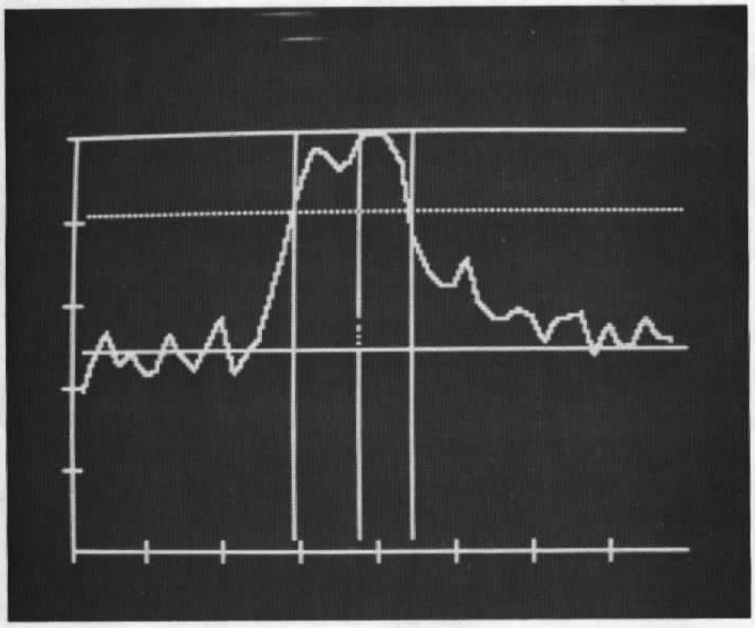

Figure C3.

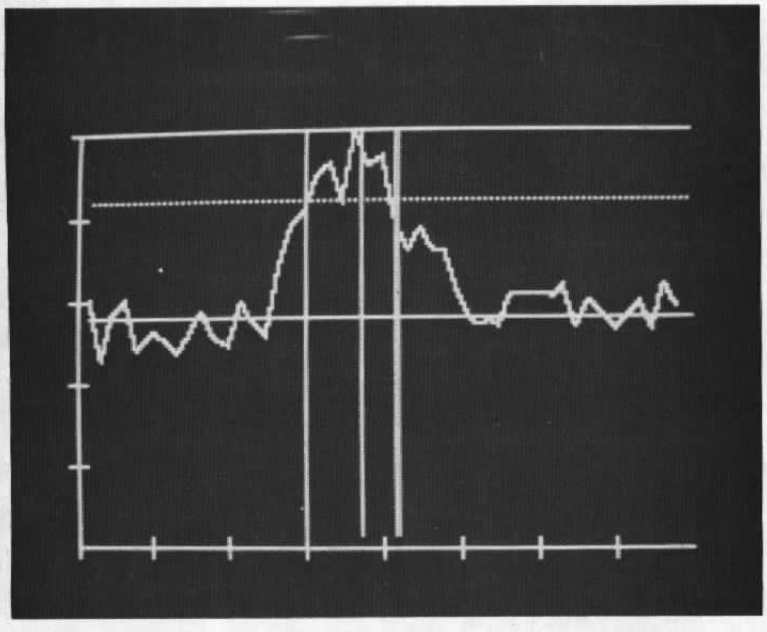

Figure C4.

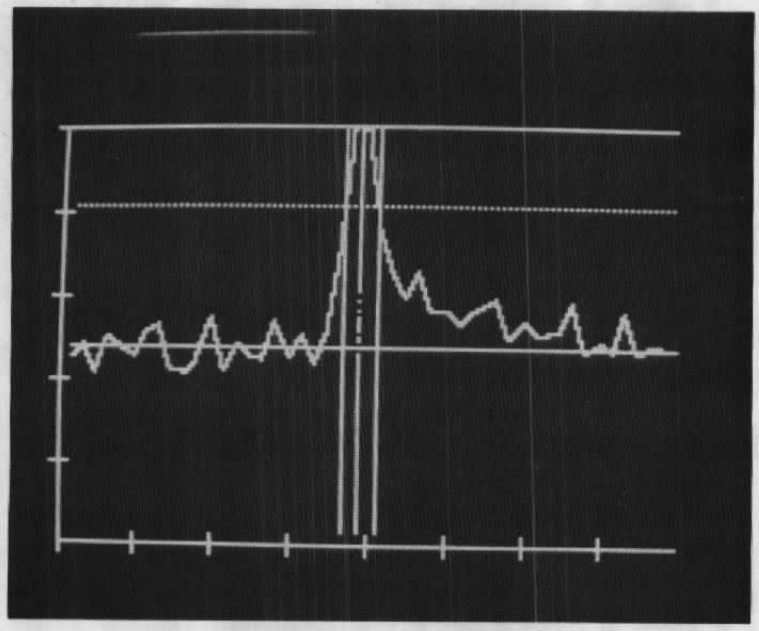

Figure C7.

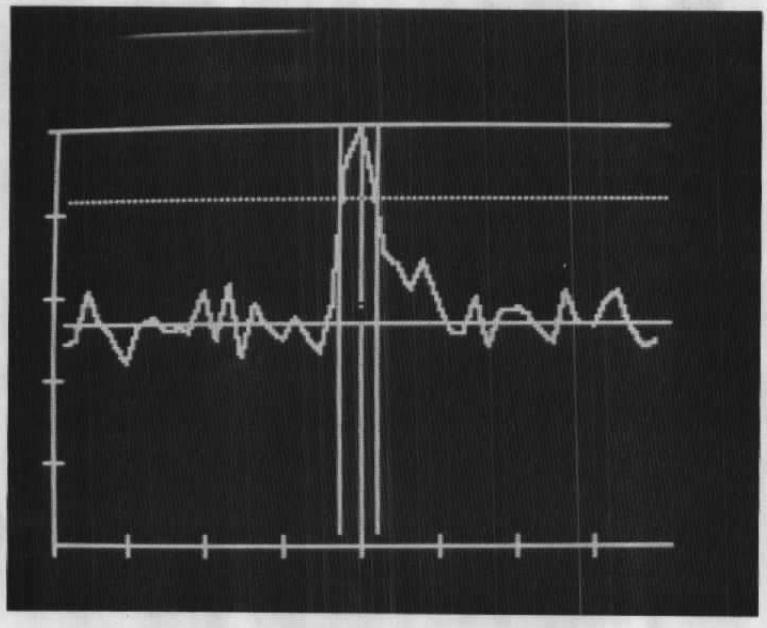

Figure C8.

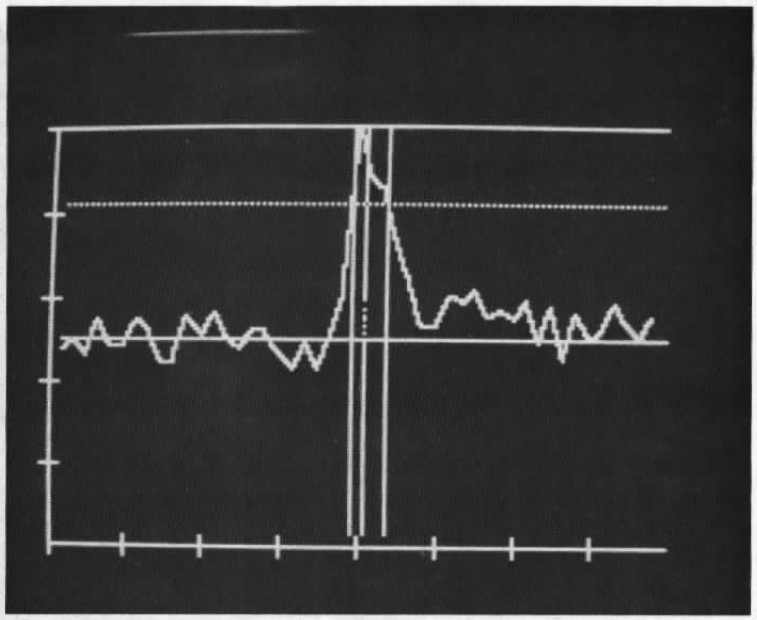

Figure C9.

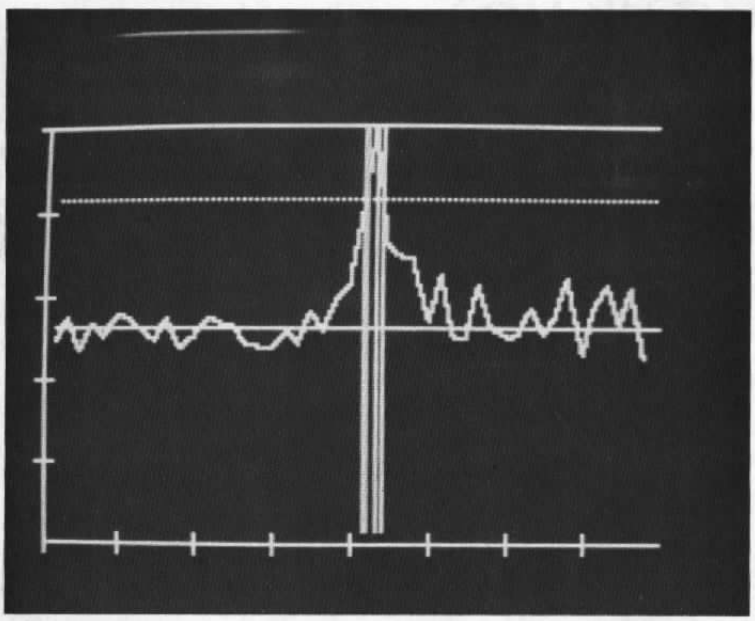

Figure C10.

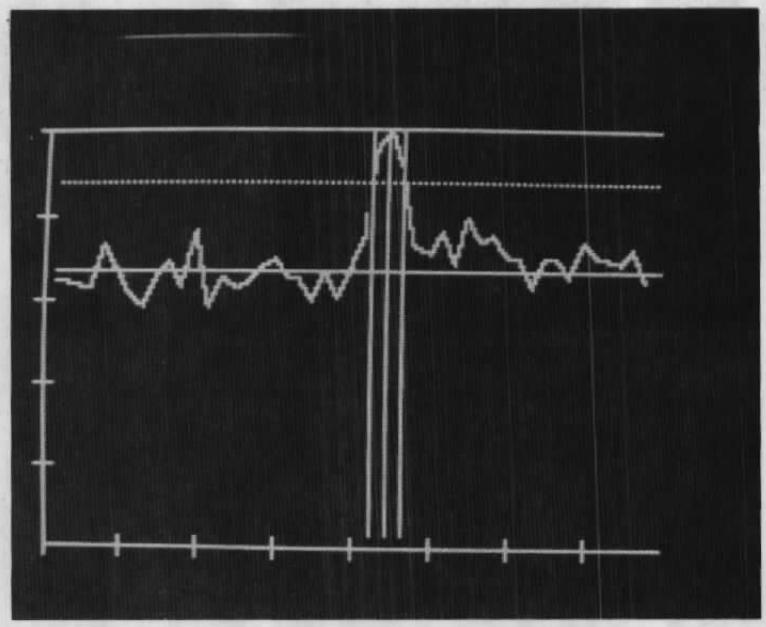

Figure C11.